AD NUMBER

AD904962

LIMITATION CHANGES

TO:

Approved for public release; distribution is unlimited.

FROM:

Distribution authorized to U.S. Gov't. agencies only; Test and Evaluation; SEP 1972. Other requests shall be referred to Air Force Avionics, Attn: TEL, Wright-Patterson AFB, Ohio 45433.

AUTHORITY

AFAL ltr, 23 Jun 1975

SUN PUMPED LASER

Lloyd Huff
GTE Sylvania, Inc.

TECHNICAL REPORT AFAL-TR-72-310

November 1972

Air Force Avionics Laboratory
Air Force Systems Command
Wright-Patterson Air Force Base, Ohio

NOTICE

When Government drawings, specifications, or other data are used for any purpose other than in connection with a definitely related Government procurement operation, the United States Government thereby incurs no responsibility nor any obligation whatsoever; and the fact that the government may have formulated, furnished, or in any way supplied the said drawings, specifications, or other data, is not to be regarded by implication or otherwise as in any manner licensing the holder or any other person or corporation, or conveying any rights or permission to manufacture, use, or sell any patented invention that may in any way be related thereto.

Copies of this report should not be returned unless return is required by security considerations, contractual obligations, or notice on a specific document.

SUN PUMPED LASER

Lloyd Huff

FOREWORD

This Final Technical Report on the "Sun Pumped Laser" summarizes the work performed on Air Force Contract F33615-72-C-1240. This effort is a continuation of the work performed under Air Force Contract F33615-70-C-1255 which covered the period from January 1970 to August 1971. This study was performed for the Avionics Laboratory, Wright-Patterson Air Force Base, Ohio and covered the period from December 1972 to July 1972. Mr. Donald D. Matulka (AFAL/TEL) was the program monitor for the Avionics Laboratory. The work was supported by the Advanced Development Program 405B. This report was submitted in September 1972.

This report was prepared by the Electro-Optics Organization of GTE Sylvania, Inc., Electronic Systems Group - Western Division, Mountain View, California, and describes work performed in the Research and Development Department, headed by Dr. L. M. Osterink. Dr. L. Huff was the project engineer for the program. Other principal contributors to the program were Mr. C. B. Hitz, Dr. G. A. Massey and Dr. J. D. Taynai. Technical assistance was provided by Mr. L. E. Wilson.

This report was submitted in September 1972 and has been reviewed and is approved for publication.

ROBERT E. DEAL, Actg Ch
Laser & E-O Tech Branch
Electronic Technology Division

ABSTRACT

This report describes the results of a program to obtain improved operating performance of the sun pumped laser developed on the previous contract, AF contract F33615-70-C-1255. With more effective cooling of the laser rod, a nearly threefold increase in the multimode output power was achieved. A multimode output power of 4.85 watts was obtained with the 24 inch diameter collector using a copper heat sink which fully contacted the circumference of the laser rod. Operation of the device in a configuration compatible with dual sun and lamp or diode pumping, was also demonstrated. Operation of the sun pumped laser in the fundamental mode was obtained with the use of an intracavity lens to expand the beam within the laser rod. A TEM_{oo} output of 0.8 watts was obtained. Mode locked operation of the laser at a pulse repetition frequency of 500 MHz was also accomplished.

TABLE OF CONTENTS

LIST OF ILLUSTRATIONS

LIST OF TABLES

Section I

INTRODUCTION

Direct use of the sun to power a Nd:YAG laser transmitter on board a communication satellite is attractive because of the potentially long operating system lifetimes made possible by this laser pumping approach. The lifetimes of conventional optical sources which may be used to pump the laser material (lamps or light emitting diodes) are currently not adequate to meet the needs of an optical communication system operating in space. Continuous operation of the communication system is desirable, however, which is not possible with exclusive sun pumping of the laser in most satellite orbits. A combination of the two pumping approaches is considered to be the optimum configuration for obtaining continuous operation of the system in addition to long lifetime. The most appropriate application of the sun pumped laser is therefore on a synchronous orbiting satellite which is occluded from the sun during only a small fraction of the orbit.

The objective of the previous sun pumped laser program (AF contract F33615-70-C-1255) was to determine the practicality of utilizing the sun pumping approach in a space operational system. The use of space compatible laser cooling techniques and efficient low order mode operation of the device had to be demonstrated before the sun pumped laser could be deemed practical for space application. Using a design which was based on conductive cooling of the laser rod and end solar pumping of the rod, a feasibility laser was fabricated and operated on this previous contract. A multimode output power of 1.65 watts was obtained from this laser using the 24 inch diameter sun collecting telescope. Mode locked operation of the multimode laser was demonstrated, although neither the pulse length nor the stability were acceptable for communication purposes. Efficient low order mode operation of the device was not obtained with this laser. The results of the contract, nonetheless, demonstrated the applicability of the design approaches used, and areas where the laser operation was being limited were identified and methods of improving the operation of the laser were suggested.

The purpose of the program reported on here was to implement the modifications identified on the previous contract to obtain improved performance of the sun pumped laser. An improved heat sink design was to be implemented which would reduce the thermal drop between the laser rod and cooling pipe and lower the operating temperature of the rod. The laser was to be operated in a configuration which was compatible with side lamp or diode pumping of the rod during solar eclipse periods. The laser resonator configuration required to obtain efficient fundamental mode operation of the device was to be determined and evaluated. Finally, stable mode locked operation of the device with short pulse duration was to be demonstrated by improving the mechanical stability of the laser and operating the laser in the TEM_{oo} mode.

Operation of the device in a configuration which is compatible with side lamp or diode pumping was demonstrated by contacting one third of the laser rod's circumference to a copper heat sink and exposing the remaining two thirds to admit the side pump light. A multimode laser output power of 1.2 watts was obtained with this scheme. This performance was inferior to that obtained on the previous contract with a niobium heat sink contacting the full circumference of the rod; therefore, a copper heat sink designed to fully contact the rod OD was implemented. A nearly three-fold increase in the multimode laser output power was achieved during this contract with the new laser rod heat sink. Using the copper heat sink fully contacting the laser rod, an output power of 4.85 watts was obtained with the 24 inch telescope. Since better performance was obtained by cooling the entire rod circumference, work with the dual pumping configuration was discontinued. Successful use of copper as the rod heat sink material indicated that, in this case, a lower rod operating temperature is more important to efficient operation than a good thermal expansion match between the rod and heat sink material. Operation of the laser in the TEM_{oo} mode was obtained with the use of an intracavity lens to expand the gaussian mode in the laser rod. A TEM_{oo} mode output power of 0.8 watts was achieved with the heat sink fully contacting the circumference of the laser rod. Mode locked operation of the laser in the TEM_{oo} mode at a pulse repetition frequency of approximately 500 MHz was also demonstrated. Improved stability and shorter pulses were obtained on this contract, however, the emphasis placed on fundamental mode operation precluded substantial improvement of the mode locked operation of the device.

Descriptions of the solar collection and relay system and the laser pumping and cooling designs are presented in Sections II and III of this report. Much of the material in these sections is contained in the final report of the previous contract[1], but it is repeated here for the convenience of the reader of this report. The analytical and experimental effort directed toward obtaining improved operation of the sun pumped laser and the results of the contract are discussed in the remaining sections of the report.

Section II

SOLAR COLLECTION AND RELAY SYSTEM

Sunlight is collected by a 24 inch diameter paraboloidal telescope mirror and transferred to the laser rod by the Cassegrainian relay system shown in Figure 1. The solar collecting telescope used for this project was provided by the Air Force as government furnished property. The primary collecting mirror is mounted in an equatorial mount with a synchronous motor clock drive which allows continuous tracking of the sun. The telescope is also equipped with vernier adjustments of the right ascension and declination axes. Small tracking errors resulting from misalignment of the telescope axis with the earth's axis can be corrected during operation with these verniers. A photograph of the solar collecting telescope with the laser apparatus mounted on the bottom of the mirror bucket is shown in Figure 2.

A description of the elements of the optical system and their position with respect to the primary mirror are given in Table I. The The secondary mirror was deposited with a dielectric overcoated evaporated silver coating which had a reflectivity of greater than 97% above 0.5μ. The aluminized primary, which was not recoated, had a measured reflectivity of 88% at 6328Å. Both the field lens and the final lens were antireflection coated with a single layer of MgF. The secondary mirror forms a virtual image of the primary at a position 3.16 inches behind the secondary. The field lens, located 21 inches from the secondary, forms a real image of the primary at the position of the final lens, 19 inches from the field lens. The object for the field lens is the virtual image of the primary formed by the secondary mirror. The final lens forms a 0.6 inch diameter solar image at the entrance of the condensing cone located 4.7 inches from the lens.

Laser experiments were performed with the silver coated secondary mirror and a "cold mirror" dielectric coated secondary mirror. The cold mirror coating was designed to reject the sun's infrared radiation above one micron, thereby reducing the heat load on the laser rod and rod cooling structure. This mirror also rejected over half of the sun's radiation in

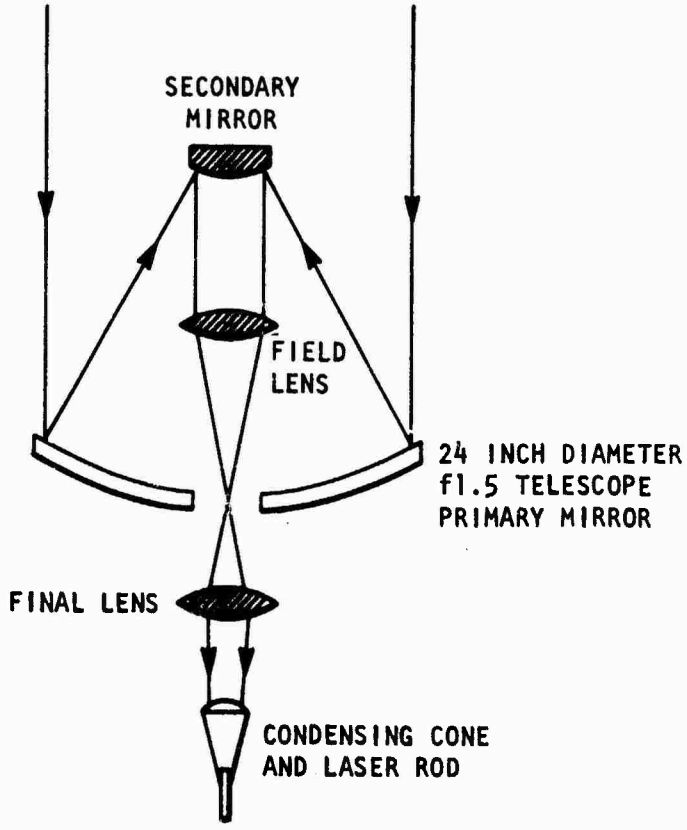

Figure 1 Solar Collection and Relay Optics

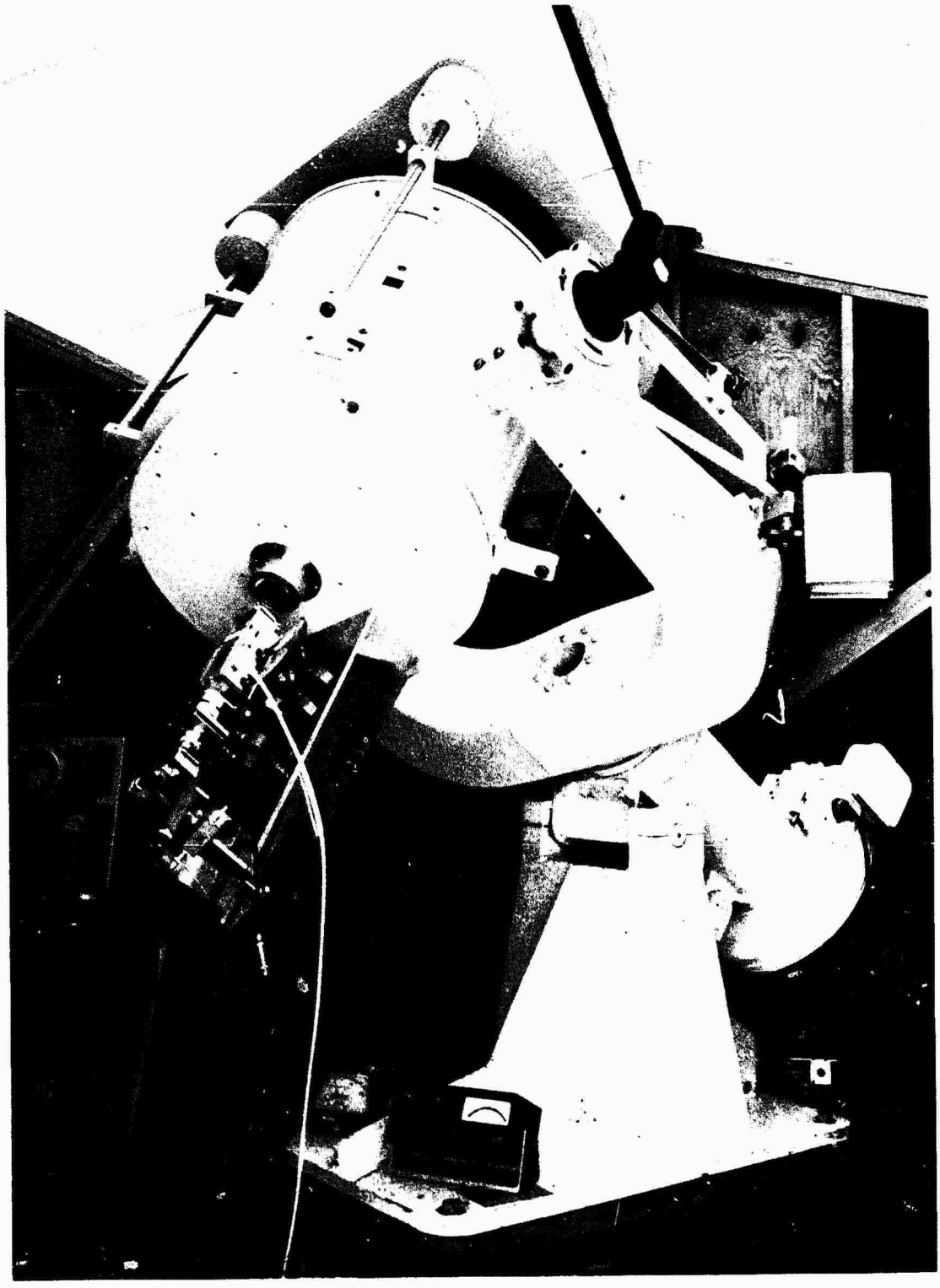

Figure 2. Sun Collecting Telescope and Laser Apparatus

Table I

Collection System Elements and Positions

Element	Description	Position
Primary Mirror	24" diameter paraboloid Focal length = 35.4"	
Secondary Mirror	3" diameter Focal length = -3.51"	33" from primary
Field Lens	3" diameter Quartz Focal length = 10.6" Antireflection Coated	12" from primary
Final Lens	3" diameter Glass Focal length = 4.0" Antireflection Coated	7" from primary

the laser rod's chromium pump band region, however, which resulted in less efficient laser operation with the dielectric mirror. The full spectrum reflectivity of the cold mirror secondary was about 45%; i.e., 45% of the total solar energy incident on the mirror was reflected. The transmission spectrum of the coating is shown in Figure 3.

An estimate of the efficiency of the collection and relay system may be obtained by multiplying the reflectivities and transmissions of the various elements. The approximate average values over the solar spectral range are:

Primary mirror	-	R = 0.88
Secondary mirror	-	R = 0.98
Field lens	-	T = 0.95
Final lens	-	T = 0.95

These values result in a collection and relay efficiency of about 78%. Taking into account the central obscuration of the secondary mirror and mount (8.5%), the efficiency is 71%; (not including the condensing cone). A summary of the power collected and relayed to the laser rod by the optical system is given in Table II for both the silver and dielectric coated secondary mirrors. The numbers given in the table were calculated using the collection and relay efficiency of 71% and a condensing cone transfer efficiency of 40%. The transfer efficiency of the cone was determined by measuring the solar power collected and relayed to the input of the cone and the power transmitted by the cone using a thermopile-type power meter. Figure 4 shows the total solar power collected by the system delivered to the cone and transferred through the cone as a function of telescope aperture. (A/A_T is the aperture area normalized to a maximum value of 1.) The aperture was varied radially by removing annular sections of fiberglass blocking the light, simulating an iris. The power relayed to the cone at full 24 inch aperture extrapolates to 145 watts, compared to a calculated power of 183 watts. The measured power is lower than the calculated power since the measurements were made at about 10:00 AM on a fairly hazy day. The calculated power value of 183 watts applies to the case of the sun at the zenith on a clear day. Referring to Figure 4, the cone transfer efficiency is about 65 percent at small aperture, and decreases to about 40 percent near full aperture. The input power to the cone is nearly linear with radial aperture; however, the cone transfer efficiency is strongly aperture dependent. Also used in the

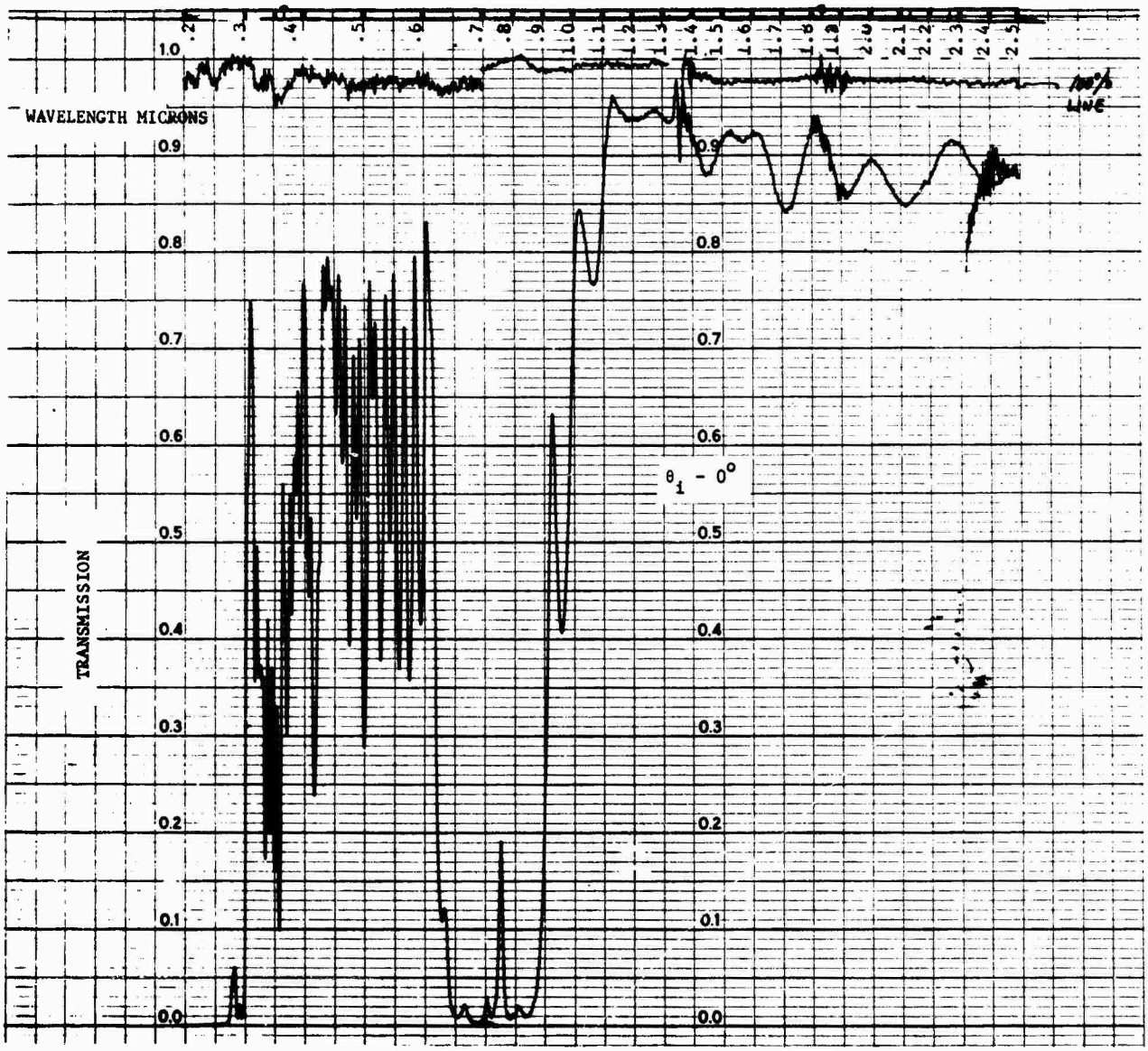

Figure 3 Transmission Spectrum of the Cold Mirror Dielectric Coating from 0.2 to 2.5 microns for normal incidence, $\theta_i = 0^0$

Table II

Power Collected and Transferred to

Laser Rod by 24-Inch Diameter Mirror

	Silver Secondary	Dielectric Secondary
Outside Earth's Atmosphere	406 watts	406 watts
At Earth's Surface (sun at Zenith)	257	257
Transferred by Optical Relay System to Cone	183	82
Transferred by Cone to the Laser Rod	75	34
Absorbed in Rod	23	14

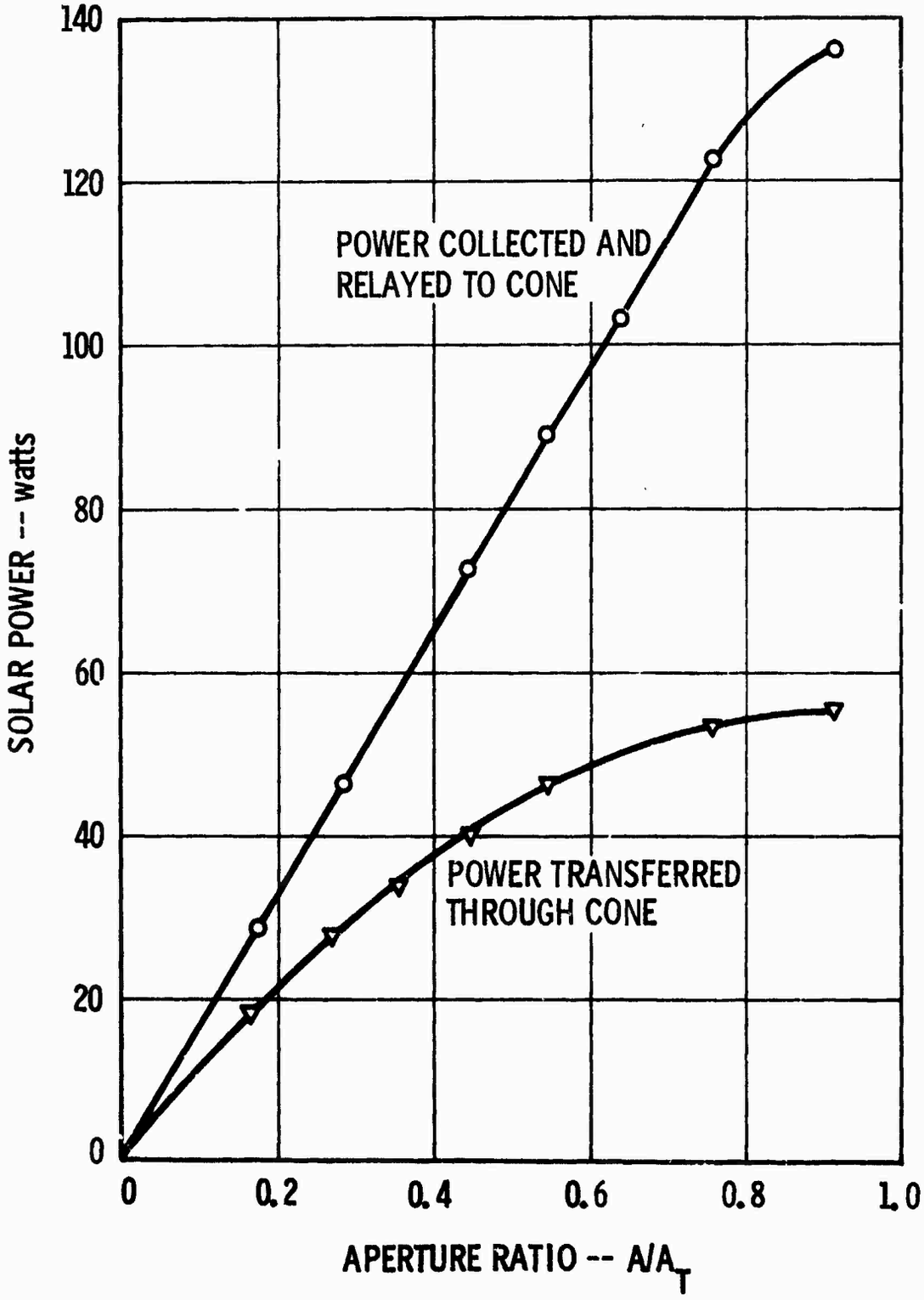

Figure 4 Total Solar Power Collected as a Function of Telescope Aperture

calculations was the fraction of sunlight absorbed by the laser rod. This was determined on the previous contract[1] to be about 30% for the silver mirror and 35% for the dielectric mirror.

A portion of the power absorbed in the rod is emitted as 1.06μ output and the remainder is dissipated in the rod as heat. Accurate information on the quantum efficiency of Nd:Cr:YAG is not available; therefore, it is not possible to accurately estimate the heat dissipation in the rod. However, based on the laser output of 4.85 watts with an estimated absorbed power of 23 watts (Table II), we estimate that at least 50% of the absorbed power is dissipated as heat.

A summary of useful solar data is presented in Table III, and the exospheric solar spectrum is given in Figure 5.

Table III

Summary of Useful Solar Quantities

1.	Solar Intensity at the outer limit of the earth's atmosphere (solar constant)	-	0.139 watts/cm^2
2.	Solar power collected by a 24" diameter mirror at the outer limit of the earth's atmosphere	-	406 watts
3.	Atmospheric transmission factor at sea level with sun at the zenith on a clear day	-	0.633
4.	Fraction of solar power above 1μ	-	27%
	Fraction of solar power below .4μ	-	13%
	Fraction of solar power in primary Nd pump bands, 0.73-0.83μ	-	9%
	Fraction of solar power in Cr pump bands, 0.38-0.65μ	-	36%
5.	Distance of sun from the earth	-	9.29×10^7 miles
	Diameter of sun	-	8.64×10^5 miles
	Angular subtense of the sun	-	9 mrad $\sim 0.5^o$

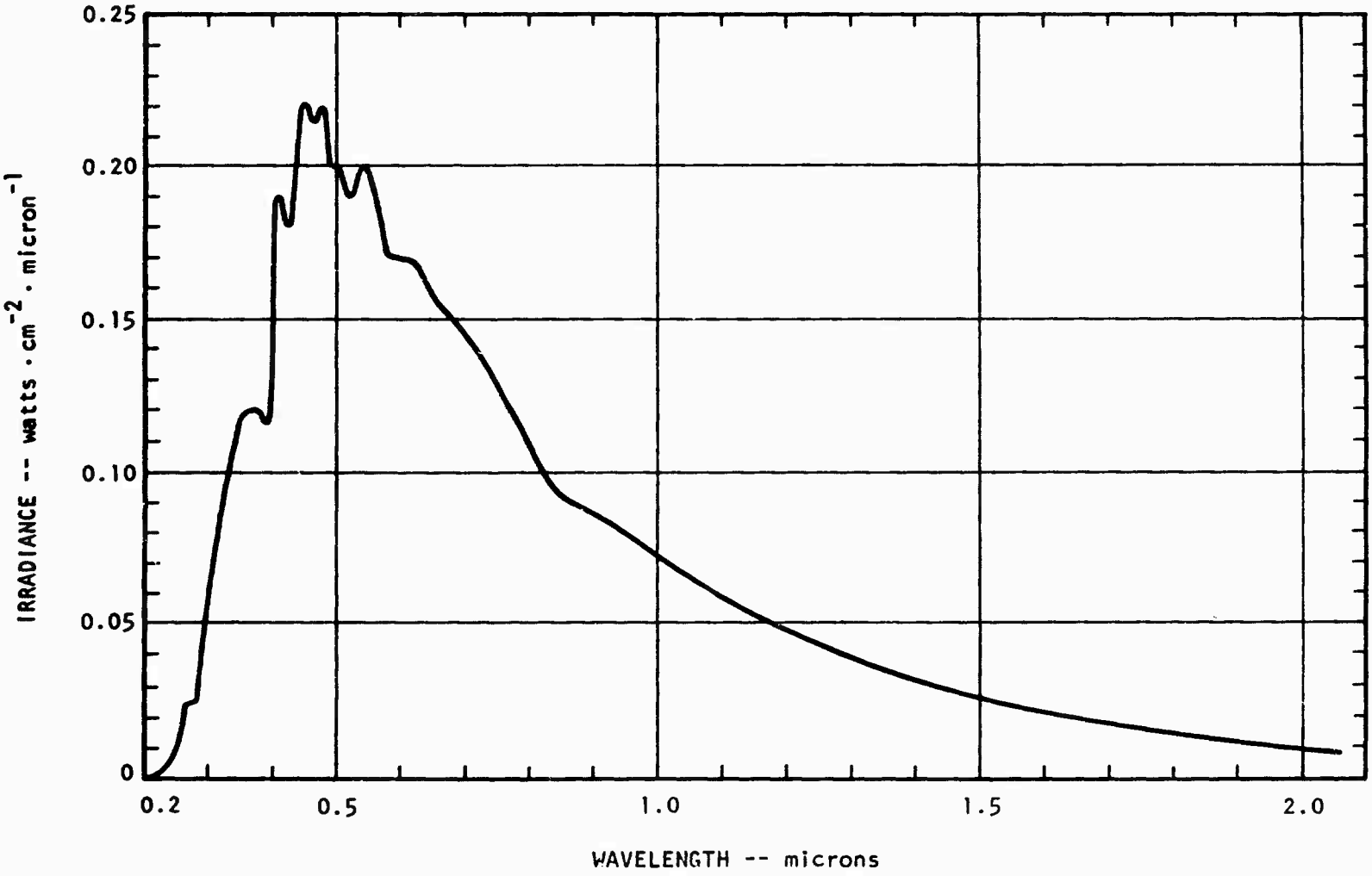

Figure 5 Spectral Distribution of Solar Radiation Outside the Earth's Atmosphere

Section III

LASER ROD PUMPING AND COOLING CONFIGURATION

1. END PUMPING OPTICS

Sunlight collected by the telescope mirror and relayed through the optical system is channeled into the end of the laser rod by a silver reflective condensing cone. A diagram of the laser is shown in Figure 6, and a photograph in Figure 7. This end pumping configuration was employed on this program for two reasons: the approach is compatible with dual pumping where the laser rod is pumped through the side by an artificial source during solar eclipse periods, and more efficient operation of the laser is believed to be realized due to the long absorption length of the rod presented to the solar pump light.

The laser material is Nd:Cr:YAG with standard Nd doping (nominally 1 atomic percent) and 0.1% doping of chromium. Transmission spectra of this material, measured on a Cary 14 spectrophotometer, are given in Figures 8, 9 and 10 (sample length = 3.3 mm). This low level of chromium doping was chosen because the optical quality of the laser material should not be impaired with the introduction of chromium at this level, and the absorption should be significant over the full length of the rod. The rod dimensions are 3 x 30 mm. The standard 30 mm rod length was used since this length should be adequate to absorb most of the solar pump light. All of these conclusions were confirmed by measurements made on the previous program. The fraction of sunlight absorbed by the laser material as a function of crystal length was measured, using the telescope and optical relay system[1]. The results of these measurements made using both the silver secondary mirror and the dielectric secondary mirror are shown in Figure 11. The experimental points were fitted by the theoretical absorption expression, $1 - T = (1 - T_f)[1 - \exp(- \langle \alpha \rangle x]$. It is observed that 70-80% of the pump light is absorbed in a one cm path length.

A condensing cone was used as the final optical element in the relay system since it provides the best means of approaching the limit of the Abbe sine condition[2]. This condition defines the smallest area into which the sunlight collected by a mirror of a given diameter can be concentrated, this limit corresponding to the theoretical minimum f number

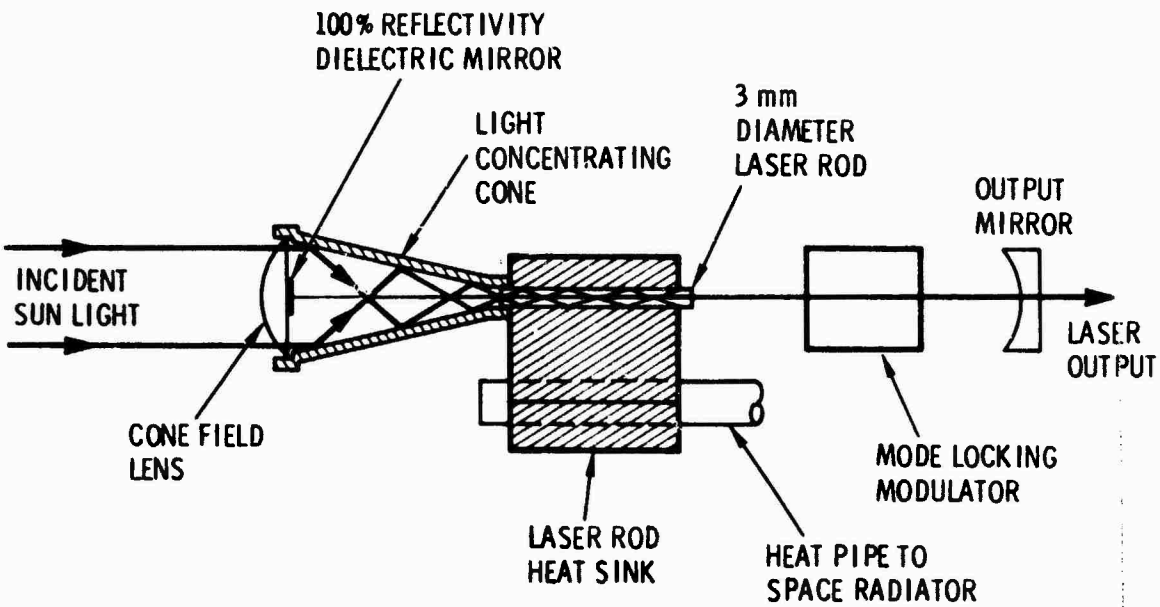

Figure 6 Sun Pumped Laser Pumping and Cooling Design

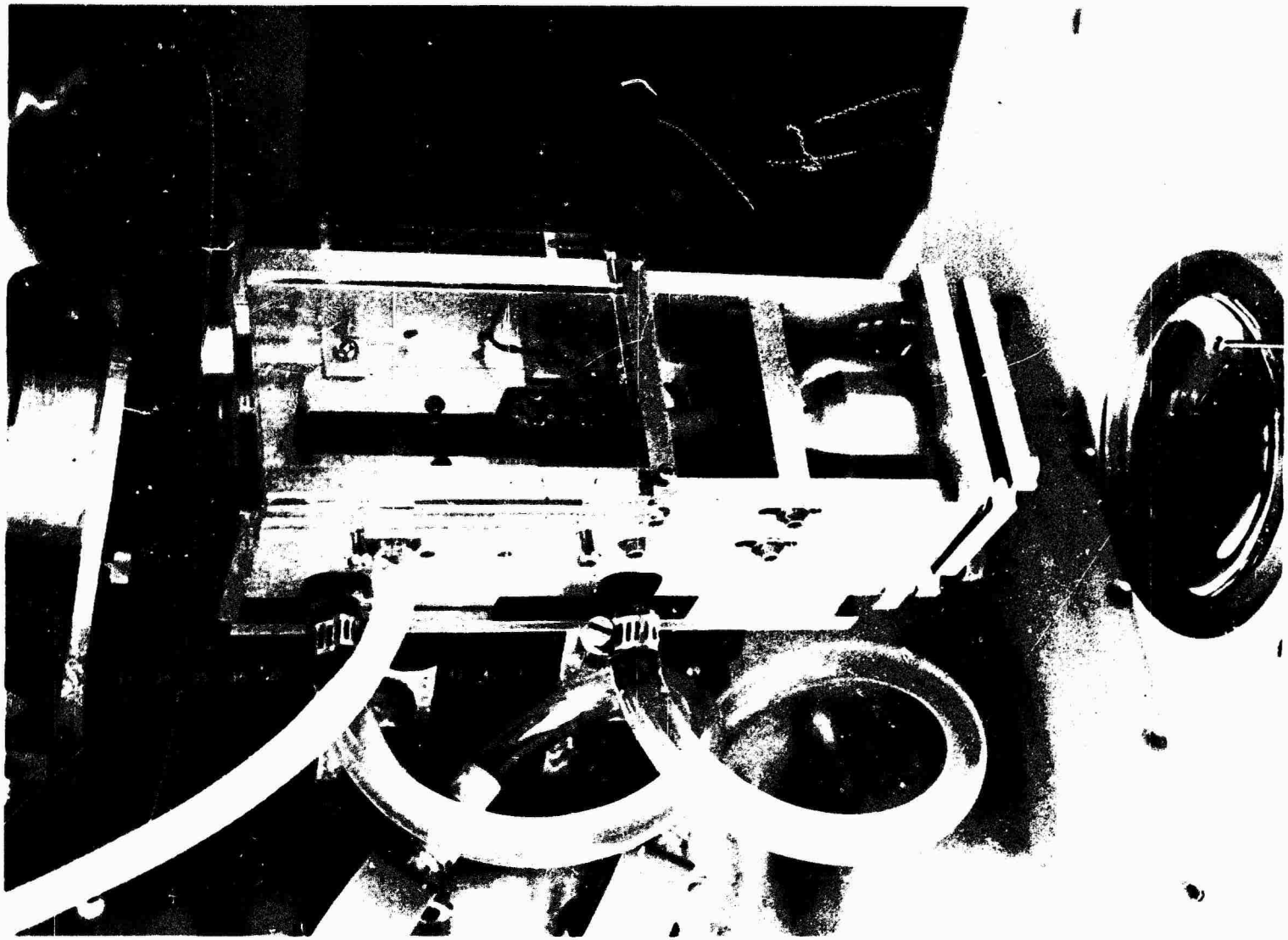

Figure 7. Sun Pumped Laser Head

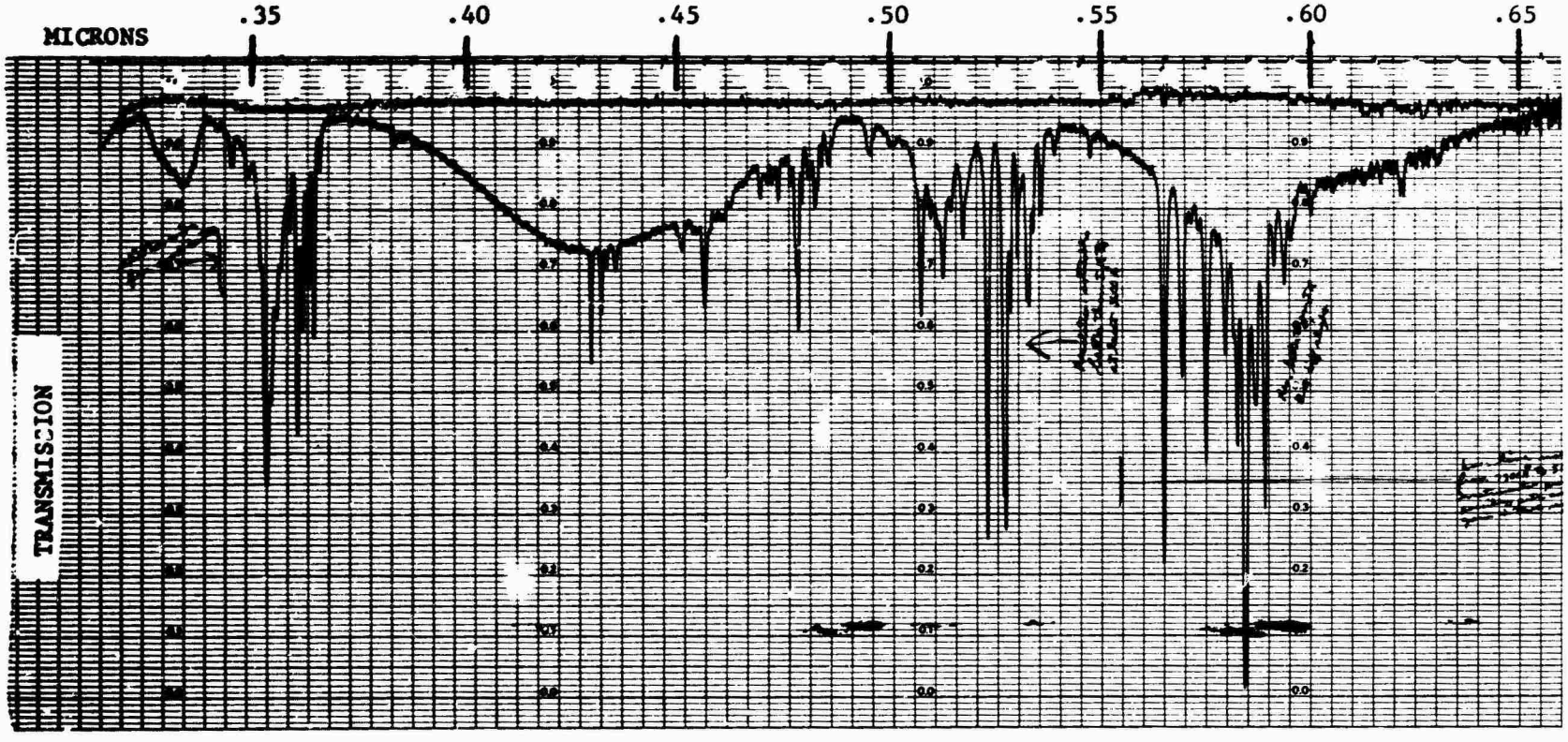

Figure 8 Transmission Spectrum of Nd:Cr:YAG from 0.35 to 0.66 microns
1% Nd, 0.1% Cr, sample length: 3.4 mm

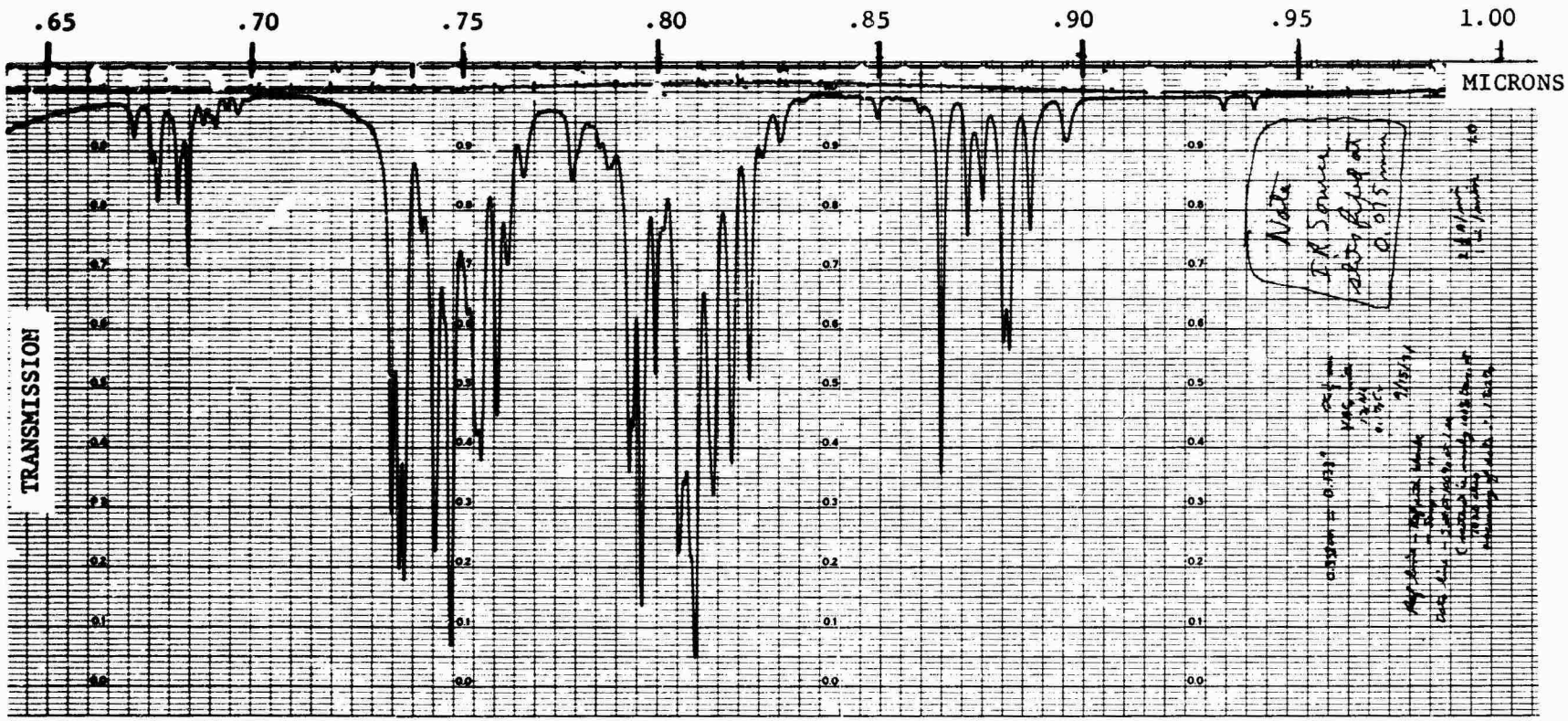

Figure 9 Transmission Spectrum of Nd:Cr:YAG from 0.65 to 1.0 micron
1% Nd, 0.1% Cr, sample length: 3.4 mm

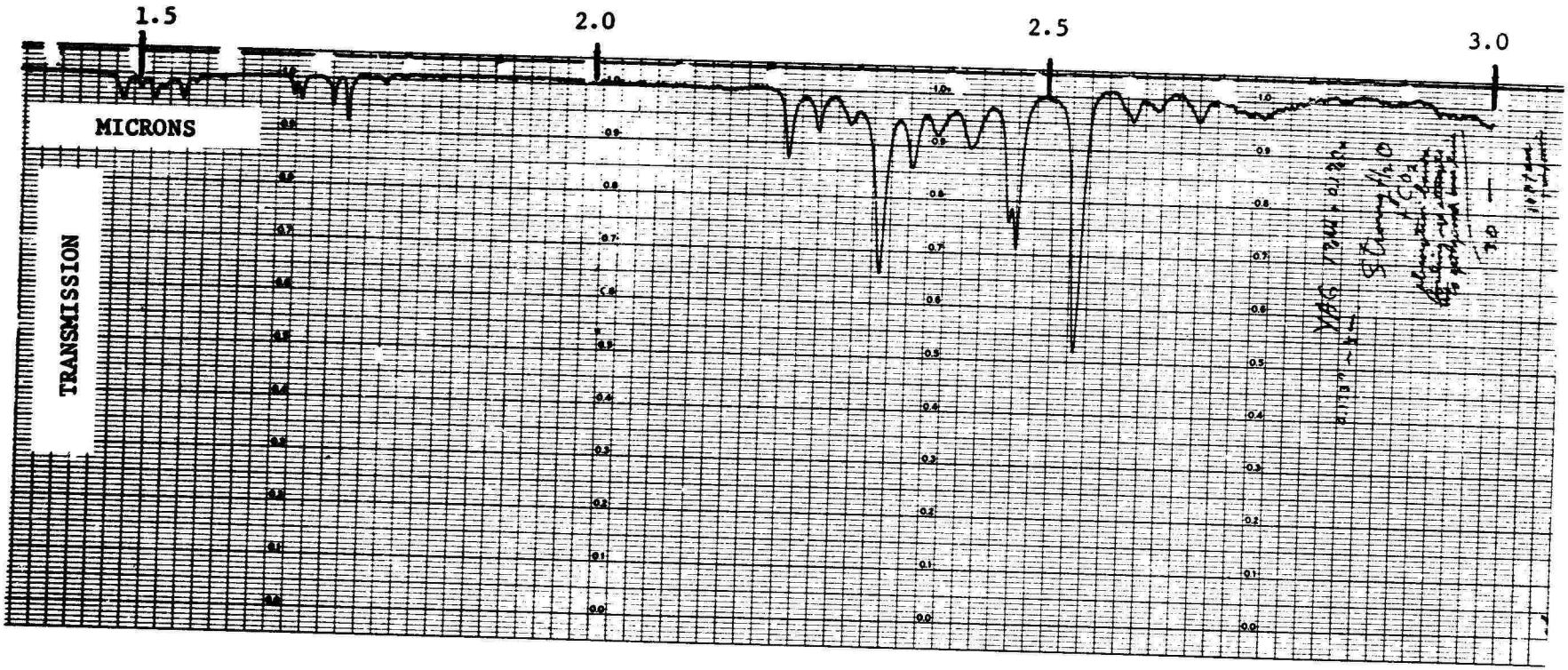

Figure 10 Transmission Spectrum of Nd:Cr:YAG from 1.4 to 3.0 microns
1% Nd, 0.1% Cr, sample length: 3.4 mm

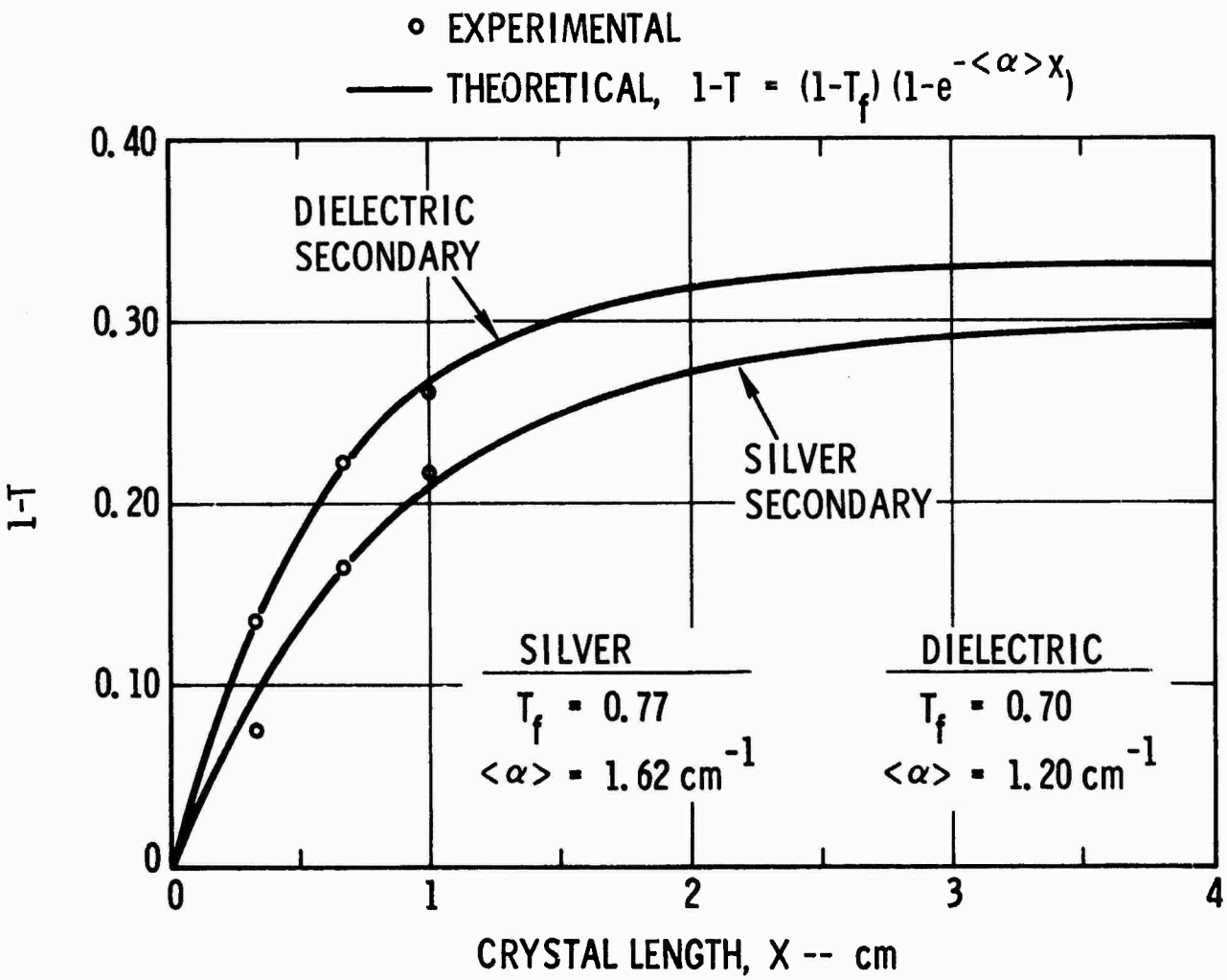

Figure 11 Fraction of Sunlight (collected by optics) Absorbed by Nd:Cr:YAG at the Earth's Surface

of 0.5. For the 24 inch diameter mirror used in this work, the Abbe sine condition limit is 2.84 mm; therefore, a 3 mm diameter rod was used. It is important that the diameter of the rod be made as small as possible in order to maximize the laser gain and allow efficient conversion to fundamental mode.

The condensing cone, shown in Figure 12, was fabricated by the electroforming process using a conical stainless steel mandrel. A layer of silver is first electrodeposited on to the mandrel and then a thick layer of copper is electroformed over the silver. Slight tarnishing of the silver surface occurred during the course of the work which was easily removed by lightly polishing the silver with lens tissue saturated with a slurry of rouge. The condensing cone is used in conjunction with a plano convex field lens (Figure 6). Both sides of this lens are antireflection coated with a single layer of MgF and the central 5 mm diameter of the plane side is deposited with the maximum reflectivity laser resonator mirror.

2. LASER ROD COOLING

The laser rod is cooled by contacting all or part of its lateral surface to a copper heat sink; the heat sink is cooled by flowing a refrigerated mixture of methanol and water through a pipe clamped to the bottom of the heat sink. The rod is bonded to the heat sink by depositing an evaporated coating onto the surface of the rod and then soldering the rod to the heat sink, using indium solder. The evaporated coating consists of layers of silver, nickel and indium. Silver is used as the base coating for its high reflectivity throughout the solar spectrum. Nickel is deposited over the silver to act as a diffusion barrier to prevent amalgamation of the indium with the silver coating during the soldering operation. Finally, a layer of indium is deposited over the nickel layer to allow ready wetting of the indium solder to the rod coating.

Pure indium solder is used because of its high ductility and low yield strength. Thermal expansion differences between the laser rod and the copper heat sink are readily absorbed in the solder layer. To further ensure that thermal stress between the rod and heat sink is minimal, stress relief slots were cut into the heat sink. Comparison of the operation of the laser with and without these slots showed, however, that their contribution is negligible with the use of the indium solder. A photograph of the rod heat sink is shown in Figure 13.

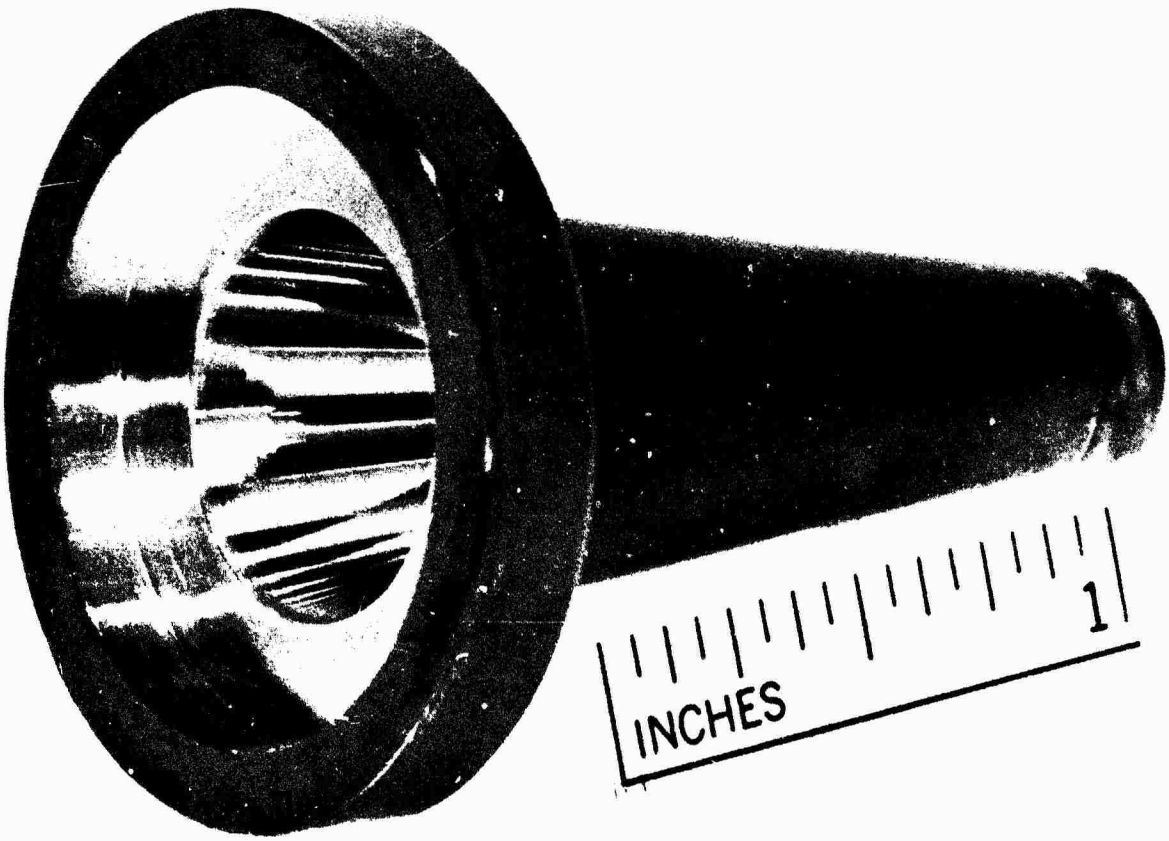

Figure 12. Electroformed Condensing Cone

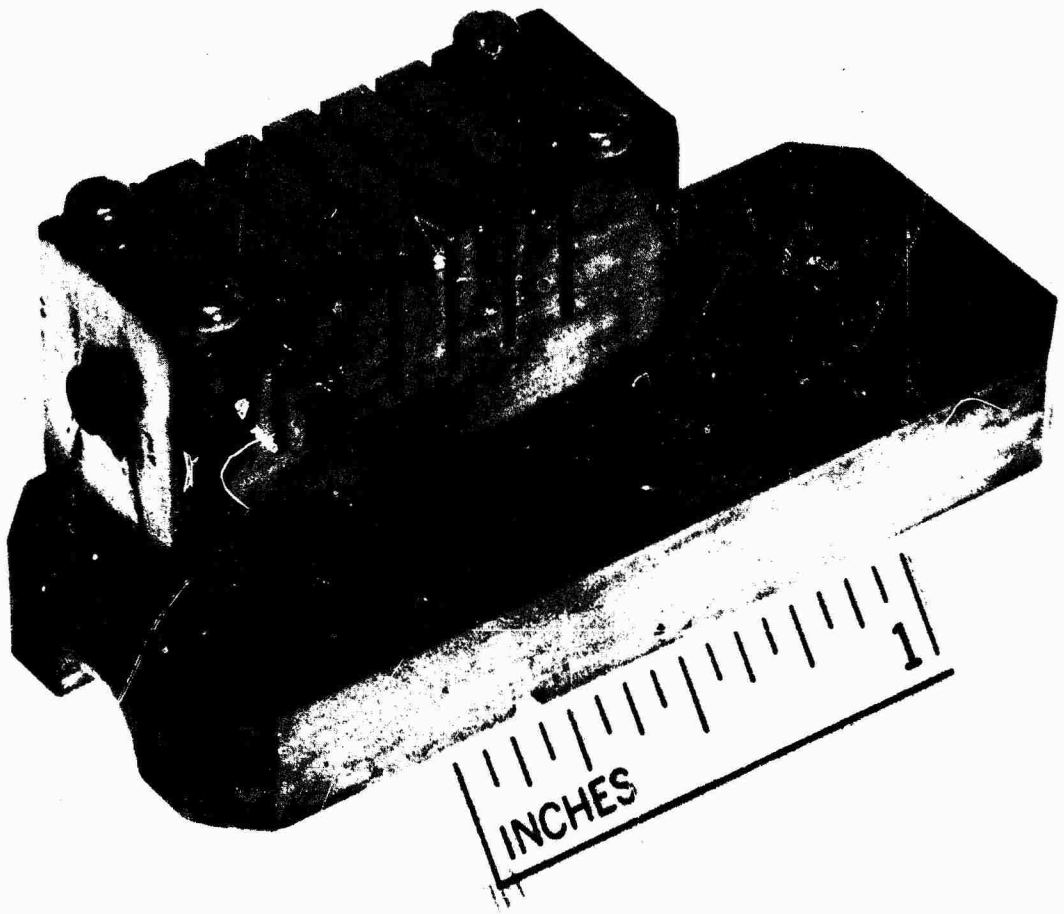

Figure 13. Laser Rod Heat Sink

Niobium was used for the heat sink material on the previous contract because of its close thermal expansion match with Nd:YAG. The thermal expansion coefficient and thermal conductivity of copper, niobium and Nd:YAG are given in Table IV. A close expansion match was believed to be necessary to prevent optical distortion in the rod caused by stress between the rod and the heat sink, even with the use of a low yield strength solder. However, the thermal conductivity of niobium is relatively low, one eighth that of copper, as seen in Table IV. Based on the performance of the laser obtained with the copper heat sink on this program it appears that minimizing the operating temperature of the rod is more important than matching the expansion coefficients of the laser rod and heat sink materials (with the use of indium solder). Greatly improved operating performance of the laser has thus been achieved with the use of copper for the heat sink material, which allows the rod to operate at a much lower temperature than with niobium.

One of the goals of this contract was to operate the laser in a configuration which was physically compatible with side lamp or diode pumping of the laser rod. This was accomplished by contacting the cylindrical surface of the rod by the heat sink over 120 degrees and leaving the remaining 240 degrees of the surface exposed to admit pump light from the artificial source. Cross sectional view of various rod heat sink configurations evaluated on this program, are shown in Figure 14. It is possible, theoretically, to operate this configuration without loss of end solar pump light, since the extreme ray from the optical system is within the critical angle for total internal reflection inside the laser rod. (This was not achieved in practice on this contract, as discussed in Section IV) The laser was also operated with the rod cooled on two opposite 120 degree sections, and with the entire circumference contacted by the heat sink. These latter cooling configurations were obtained by depositing the evaporated coating over the full lateral surface of the rod, and placing a cap over the rod as shown in Figure 14. The rod is soldered to both the wedge and the cap for these cases.

Table IV

THERMAL PROPERTIES OF COPPER, NIOBIUM AND Nd:YAG

Material	Thermal Expansion Coefficient (at room temperature)	Thermal Conductivity (at room temperature
Copper	16.8×10^{-6} $^{o}C^{-1}$	4.00 watts$\cdot cm^{-1} \cdot {}^{o}K^{-1}$
Niobium	7.1×10^{-6}	.52
Nd:YAG	6.9×10^{-6}	.13

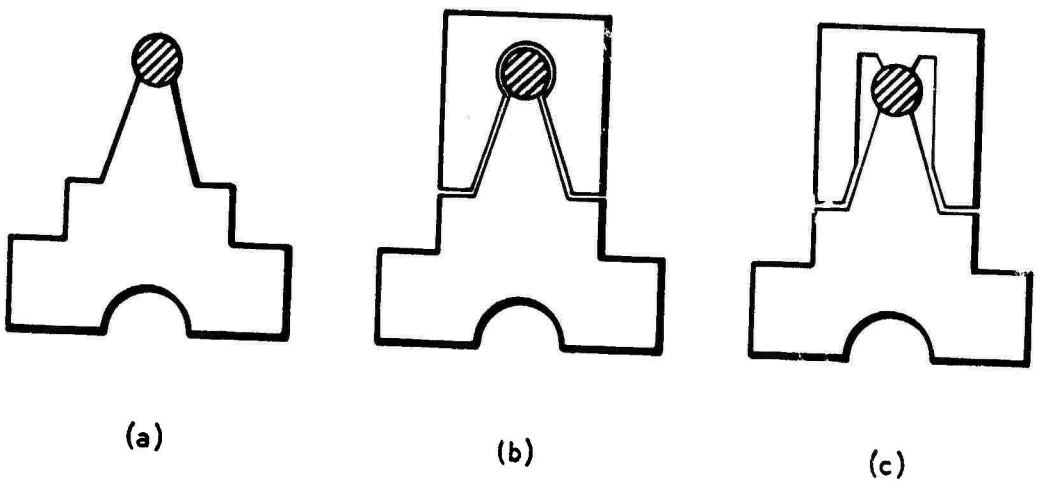

Figure 14 Cross Sectional Views of Various Rod-Heat Sink Configurations (a. - One third of rod contacted by heat sink; b. - Rod circumference fully contacted by heat sink; c. - Rod contacted by heat sink on two opposite 120° sections)

Section IV

LASER OPERATION WITH VARIOUS ROD-HEAT SINK CONFIGURATIONS

1. DUAL PUMPING CONFIGURATION

Operation of the end sun pumped laser in a configuration compatible with side lamp or diode pumping of the laser rod during solar eclipse periods was accomplished using the rod-heat sink assembly shown in Figure 14a. One third of the rod's cylindrical surface was contacted to the heat sink and the remaining two thirds was exposed to admit the pump light from an artificial source. The laser was operated using both the silver secondary and the dielectric secondary mirrors.

The performance of this rod-heat sink configuration is shown in Figure 15. The multimode laser output power is plotted as a function of the fraction of the telescope aperture area opened to the sunlight. The quantity A/A_T is the exposed primary mirror area divided by the total mirror area available, taking into account the central obscuration of the secondary mirror and mount ($\sim$ 9%). For this graph the telescope is opened radially by removing a set of aperture rings. Also shown in Figure 15 is the multimode performance of the laser obtained on the previous contract with the laser rod's cylindrical surface fully contacted by a niobium heat sink.

The temperature of the heat sink wedge about 0.025 inch from the rod's cylindrical surface, and about 0.075 inch from the input end of the rod, was monitored with an iron-constantan thermocouple. This temperature, which should be close to the skin temperature of the rod, at this axial rod position, is indicated by the number next to each experimental point in Figure 15. The refrigeration unit used to chill the coolant fluid was operated at its maximum capacity during these experiments, and no attempt was made to maintain a constant rod temperature as the telescope aperture area was varied.

The multimode performance of the laser, with one third of the rod contacted by the copper heat sink, is observed to be superior to that with the rod fully contacted by the niobium heat sink, at low values of A/A_T,

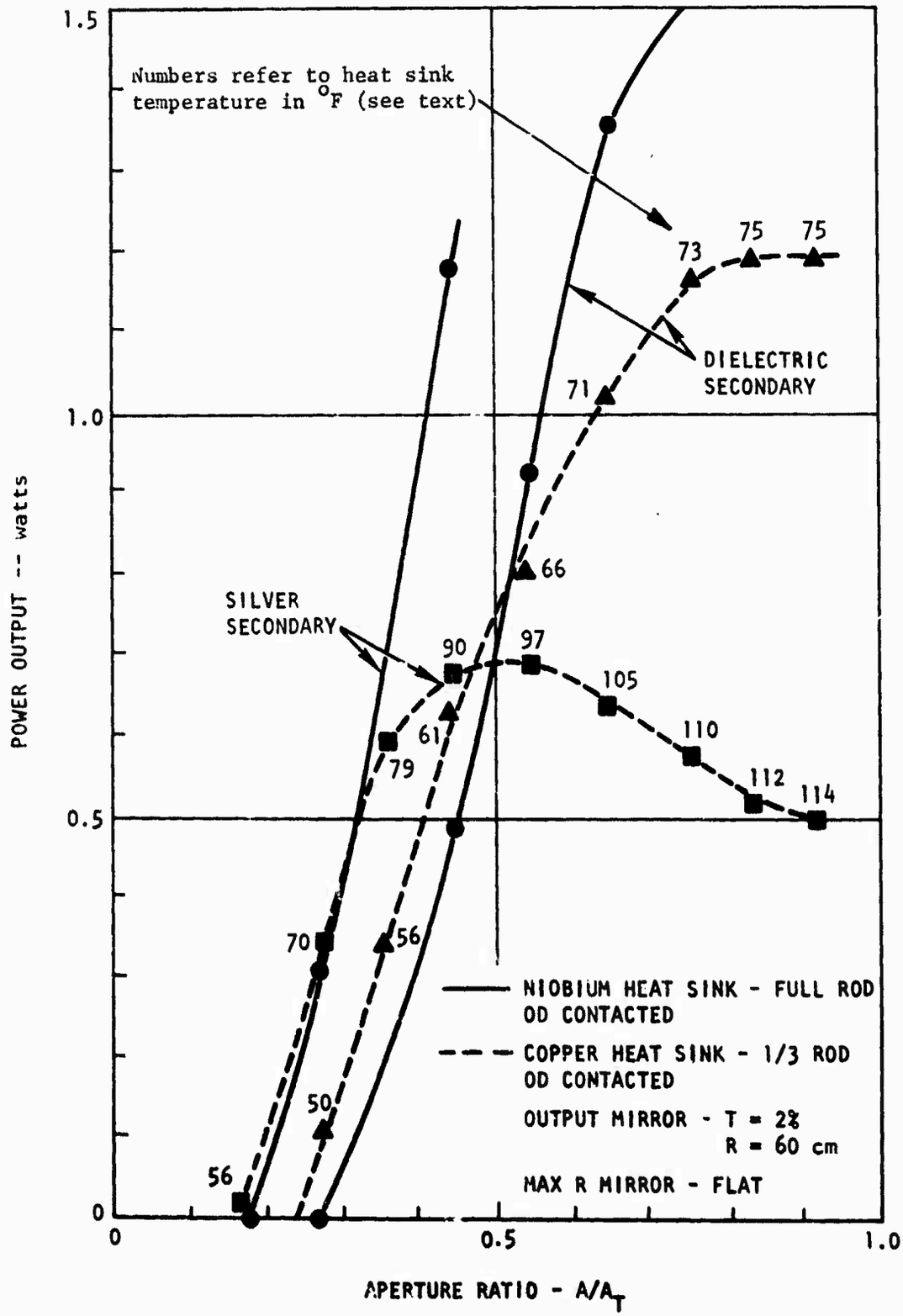

Figure 15 **Laser Performance With One Third of Rod Cooled Compared to Previous Contract Results**

but the reverse is true at high values of A/A_T. In fact, the output with the silver mirror saturates and decreases for values of A/A_T greater than 0.5. The behavior of the laser with this copper heat sink configuration, is due to two effects: (1) less effective cooling of the laser rod with only one third of the rod contacted by the heat sink and (2) loss of pump light due to scattering at the exposed lateral surface of the rod.

A ray trace of the extreme ray transferred by the condensing cone and entering the laser rod shows that the bounce angle of this ray, within the rod, is greater than the critical angle for total internal reflection and, therefore, should be trapped. No loss of pump light should occur, then, if the cylindrical surface of the rod is highly polished. Microscopic examination of the laser rod revealed this surface to have a relatively rough finish, however, rather than a low scatter optical polish. Thus, as the telescope is opened, pump light is incident on the surface of the rod at steeper angles, and an increasing amount of light is scattered through the surface and lost. This effect was observed visually, although no effort was made to measure the pump light loss quantitatively.

Although this pump light loss contributes to the observed behavior of the laser, the dominant effect is undoubtedly the increased heat load on the rod. The surface temperature of the rod at the heat sink increased as the telescope was opened, since the cooling system was operating at maximum capacity, and the increased rod temperature caused the output power to be reduced at the higher pump levels. Had this temperature been maintained constant, the saturation of the output would not have been as pronounced. The maximum heat sink temperature of 114°F for the silver mirror operation, and 75°F for the dielectric mirror operation with the partially contacted copper heat sink, compare to a temperature of approximately 100°F for silver and dielectric mirror operation with the fully contacted niobium heat sink. (The previous silver mirror operation with the niobium heat sink was limited to $A/A_T = 0.5$ in order to maintain this temperature.) The heat sink temperatures with the silver mirror are comparable for the two heat sink configurations; with the dielectric mirror the temperature of the copper heat sink is lower. The reduced laser

output, with the partially contacted laser rod and telescope fully open, is due primarily to the increased thermal gradient across the rod. We can readily estimate the magnitude of this gradient by solving the heat flow equation for the case of a square cross-section laser rod cooled on one face. This will not give the exact gradient for the case of the round rod, but it should be a good approximation. Analytically treating the case of a round rod cooled on one third of its circumference is a much more difficult problem and was beyond the scope of this program. The heat flow equation for the square geometry, assuming uniform heat generation within the rod, is

$$\frac{\partial^2 T(x)}{\partial x^2} = -\frac{h}{k} \tag{1}$$

where h = heat generation rate
k = thermal conductivity

The geometry is depicted in Figure 16. The solution of this equation is

$$T(x) = -\frac{h}{k} x^2 + \frac{\Delta T}{d} + \frac{hd}{2k} + T_1 \tag{2}$$

Since the temperature gradient is zero at x = d, we have

$$-\frac{h}{k} x \Big|_{x=d} + \frac{\Delta T}{d} + \frac{hd}{2k} = 0 \tag{3}$$

$$\Delta T = \frac{hd^2}{2k} \tag{4}$$

It is observed from Figure 11 that 70-80% of the pump light is absorbed in the first cm length of the laser rod. For the silver mirror it is estimated that the amount of power absorbed by the rod is about 35 watts. If we assume that half of the absorbed power is converted to 1.06 micron fluorescence, the amount of heat dissipated by the rod is then 17.5 watts. (As we mentioned earlier, accurate information on the quantum efficiency of Nd:Cr:YAG is not available.) Considering this heat to be generated uniformly within

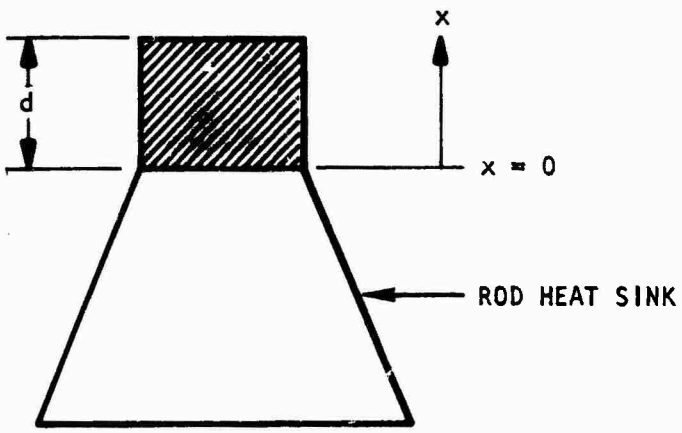

Figure 16 Geometry for Rod ΔT Calculation

the first cm of the rod, the heat generation rate is

$$h = \frac{17.5}{\pi \left(\frac{0.3}{4}\right)^2 (1)} = 248 \text{ watts/cm}^3$$

Let us approximate the round 3 mm diameter rod with 120° of its surface cooled by a square rod 2.5 mm on a side cooled on one face. The ΔT across the rod is then calculated to be

$$\Delta T = \frac{(248)(0.25)^2}{(2)(0.14)} = 55^\circ C = 99^\circ F$$

The exposed surface of the rod opposite the heat sink is thus estimated to be at a temperature of $99 + 112 = 211^\circ F$. A point on the surface of the rod near the input end will be hotter than this since the absorption of the pump light is exponential and not uniform.

For the case of the round rod cooled on its entire periphery, the highest temperature is on the rod axis. The ΔT between the surface and axis of the rod may be calculated in a similar manner. For this case the heat flow equation is

$$\frac{\partial^2 T(r)}{\partial r^2} + \frac{1}{r}\frac{\partial T(r)}{\partial r} + \frac{h}{k} = 0 \qquad (5)$$

solution of the equation yields

$$\Delta T = \frac{1}{4}\frac{h}{k} r_o^2 \qquad (6)$$

where r_o is the radius of the rod. Assuming the same heat generation rate as above we find for this cooling configuration

$$\Delta T = \frac{1}{4}\frac{248}{(.14)}(.15)^2 = 16^\circ C = 29^\circ F$$

This value of ΔT is roughly one third of that for the rod cooled on one third of its surface as we would expect. It is primarily this smaller temperature gradient within the rod which accounts for the superior performance of the rod with the entire cylindrical surface contacted by the heat sink.

Since the primary goal of the program was to obtain efficient operation of the device in the TEM_{oo} mode, effort to operate the laser with dual pumping compatibility was discontinued. In order to achieve the required mode locked performance in the TEM_{oo} mode, a multimode power of at least two to three watts would be required; the output power of 1.2 watts, obtained with the heat sink configuration discussed above, was not sufficient. These results do not mean that dual pumping is not practical. There are other configurations which do not have the disadvantages displayed by the one described here, and would likely exhibit efficient performance in both sun and lamp or diode-pumped modes of operation. One such configuration involves pumping different portions of the rod with the sun and the auxiliary source. In this approach, the sun pumped portion of the rod is fully contacted by the heat sink and the remaining lamp pumped length is contacted to the heat sink over one third of the rod periphery. This approach to lamp pumping and cooling the laser rod has proved successful. Figure 17 shows the laser performance of the rod-heat-sink configuration of Figure 14a, pumped by a krypton arc lamp in an elliptical pump cavity. The same 3 x 30 mm Nd:Cr:YAG rod used in the sun pumped laser experiments, was used for this lamp pumped experiment. In the lamp pump experiment, the entire length of the rod was pumped by a 1.2 inch arc length lamp. Another possibility is to completely separate the two pumping mode by providing two separate laser heads in the system, one sun pumped and the other lamp pumped. This ultimately may be the most effective way of achieving continuous operation of the laser system since independent optimization of both operating modes may be necessary to obtain the maximum performance. A system trade-off study of the advantages and disadvantages of the single head and dual head approach is required to determine the optimum approach.

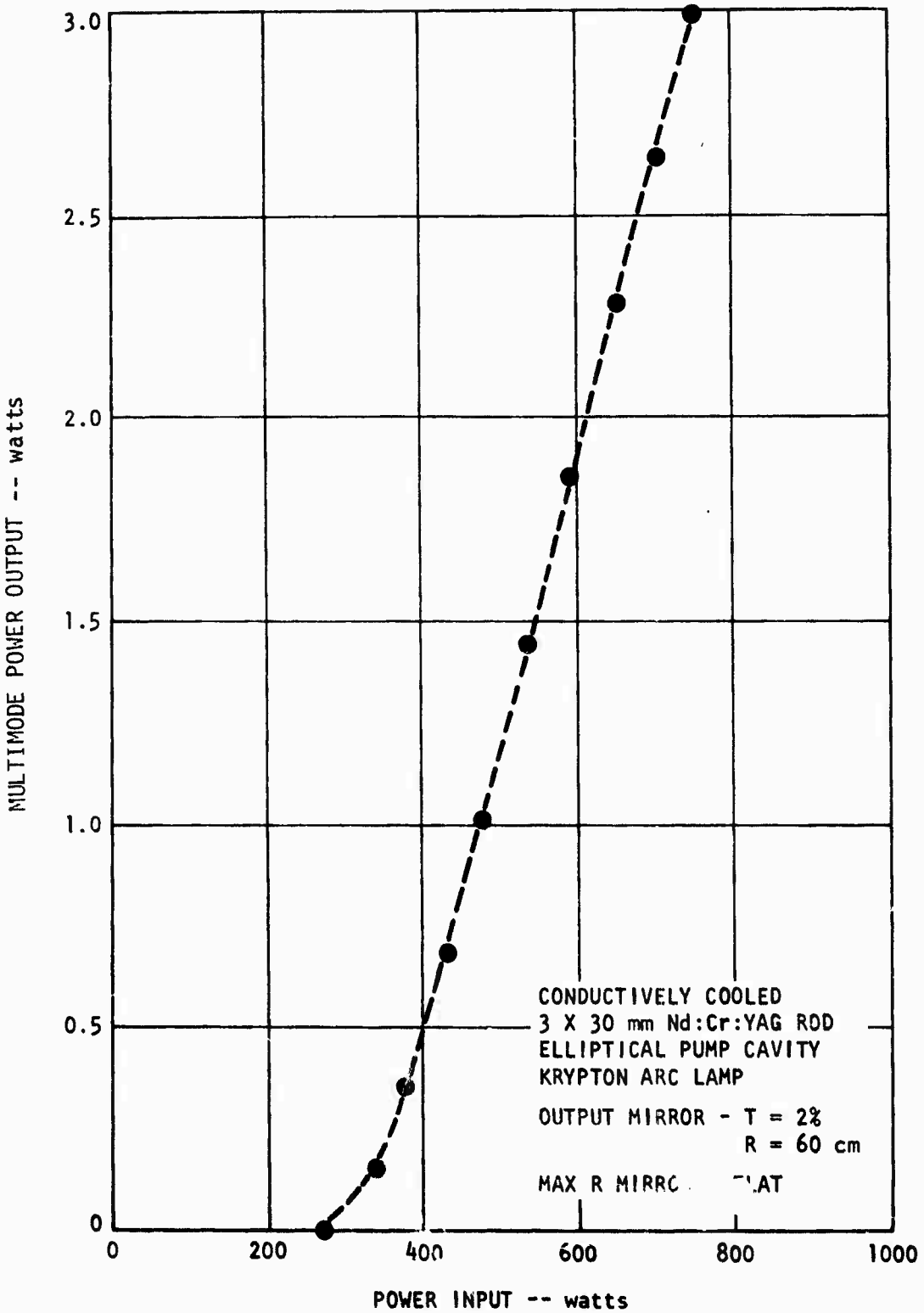

Figure 17 Lamp Pumped Laser Performance of the Dual Pumped Rod-Heat Sink Configuration

2. FULL CIRCUMFERENTIAL ROD COOLING

The results of the experiments described in the previous section indicated that improved multimode operation of the laser could be obtained by cooling the entire circumference of the rod with the copper heat sink. The cooling configuration shown in Figures 13 and 14b was therefore implemented. The evaporated coating was applied to the full periphery of the rod, and a copper cap was placed over the heat sink wedge to contact the remaining two thirds of the rod's surface.

The multimode performance of the laser with this rod cooling scheme, is shown in Figure 18. Superior operation of the laser is, indeed, obtained with no saturation of the laser output for both the dielectric and silver secondary mirrors. The decrease in the laser slope efficiency at the higher value of A/A_T is due to the decrease in the transfer efficiency of the optical relay system as the telescope aperture (mirror) diameter increases. This effect is discussed in more detail in Section IV. A multimode output power of 4.3 watts was obtained from the laser during these experiments; a power of 4.85 watts was achieved later with a new condensing cone.

The temperature of the heat sink cap was monitored with an iron-constantan thermocouple located about 0.050 inches from the surface of the rod near the input end of the rod; the temperature of this point should be close to the surface temperature of the rod. The temperature of the base of the heat sink was also measured. With the telescope fully opened the following temperatures were recorded:

Silver Secondary	Dielectric Secondary
$T_{cap} = 81^{\circ}F$	$T_{cap} = 55^{\circ}F$
$T_{base} = 41$	$T_{base} = 33$
$\Delta T = 40^{\circ}F = 22^{\circ}C$	$\Delta T = 22^{\circ}F = 12^{\circ}C$

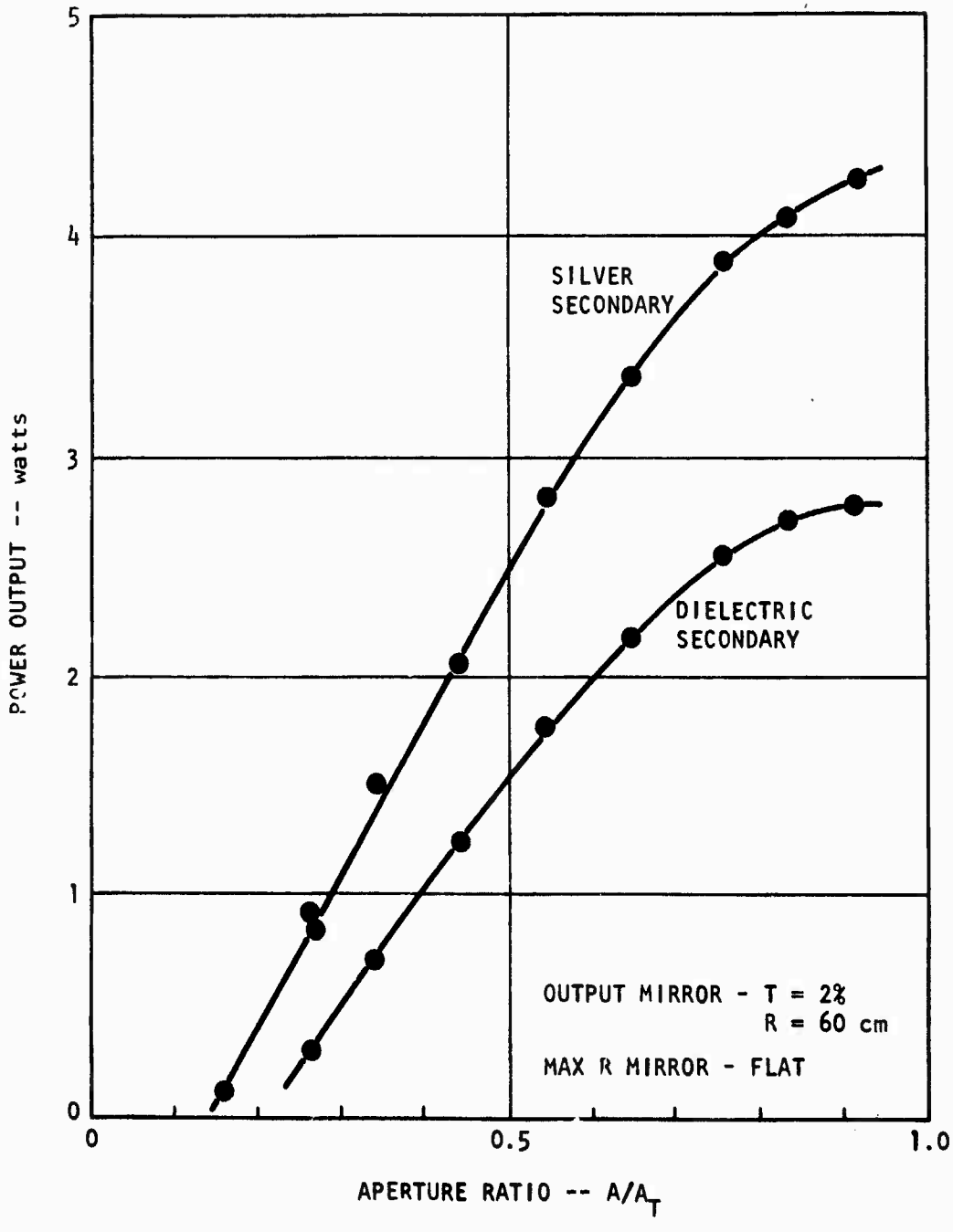

Figure 18 Sun Pumped Laser Performance With the Rod Circumference Fully Contacted by the Heat Sink

The temperature drop across the heat sink with the silver secondary is about twice that for the dielectric secondary as expected, since the dielectric secondary reflects 45% of the total sunlight incident on it, and the fractions of light reflected from these two mirrors absorbed in the rod are about the same. An estimate of the heat dissipated in the laser rod can be derived from these temperature measurements. An accurate value of the thermal resistance of the heat sink cannot be calculated simply because of the non-uniform pump absorption in the rod, and the complicated geometry of the heat flow. We will greatly simplify the problem by assuming that the pump absorption and heat flow is distributed uniformly along one half of the length of the rod and heat sink. Making this assumption, the thermal resistance of the heat sink is calculated to be 0.4 ^{o}C/watt. Using this value of thermal resistance and the measured values of ΔT above, we find the heat dissipated by the heat sink to be

Silver Mirror	Q = 55 watts
Dielectric Mirror	Q = 32 watts

These values of heat dissipation are higher than the amounts we deduce from the powers absorbed in the rod given in Table II. If we assume that one half of the pump absorption is converted to 1.06 micron fluorescence, the rod heat dissipation from Table II is 11.5 watts for the silver mirror, and 7 watts for the dielectric mirror. The discrepancy between the heat dissipation values derived by the two means can be accounted for, in part, by the absorption of the silver coating on the rod, which is typically about 5%. It is clear, however, that a more sophisticated analysis of the heat flow is required to obtain an accurate estimate of the heat dissipated by the laser rod.

3. ROD COOLED ON TWO OPPOSITE 120^{o} SECTIONS

Fundamental mode experiments performed with the fully contacted laser rod, which are discussed in Section VI, were successful in converting 10-15% of the available multimode power to the TEM_{oo} mode. This conversion efficiency compares to values of 30-50%, which were observed for lamp pumped

conductively cooled lasers on the Space Laser Design contract.[3] These lasers differ, of course, in both pumping and cooling geometries. One possible explanation for the superior TEM_{oo} mode performance of the lamp pumped laser was that this behavior was due to the asymmetrical cooling of the lamp-pumped rod. Such a cooling geometry leads to an approximately cartesian thermal distribution within the rod. Depolarization loss, due to thermal birefringence, is smaller for the cartesion geometry than for the circular profile of a radially-cooled rod. Superior operation of the laser in the TEM_{oo} mode might, therefore, be obtained with the rod cooled on one third of its circumference. Sun pumped laser operation of this configuration had exhibited poor multimode efficiency, however. In order to take the presumed advantage of the cartesian cooling geometry, and still cool the rod effectively, a heat sink designed to cool the rod on two opposite 120^{o} sections, was prepared (Figure 14c), and a second 3 x 30 Nd:Cr:YAG rod of the same doping as the previous rod was coated and soldered into the heat sink. The multimode performance of this cooling arrangement, compared to the previous scheme, is shown in Figure 19. The output power lies between that for the cases of one third circumference, and full circumference cooling, indicating that heat removal from the rod is improved over that for the heat sink contacting one third of the rod, although still not adequate (at least for operation with the silver secondary).

Operation of this heat sink arrangement with the dielectric mirror and evaluation of its TEM_{oo} mode behavior was prevented by fracture of the laser rod during one of the multimode tests. The portion of the rod protruding into the condensing cone was improperly positioned; contact of the rod and cone resulted in stresses during operation which were sufficient to break the rod.

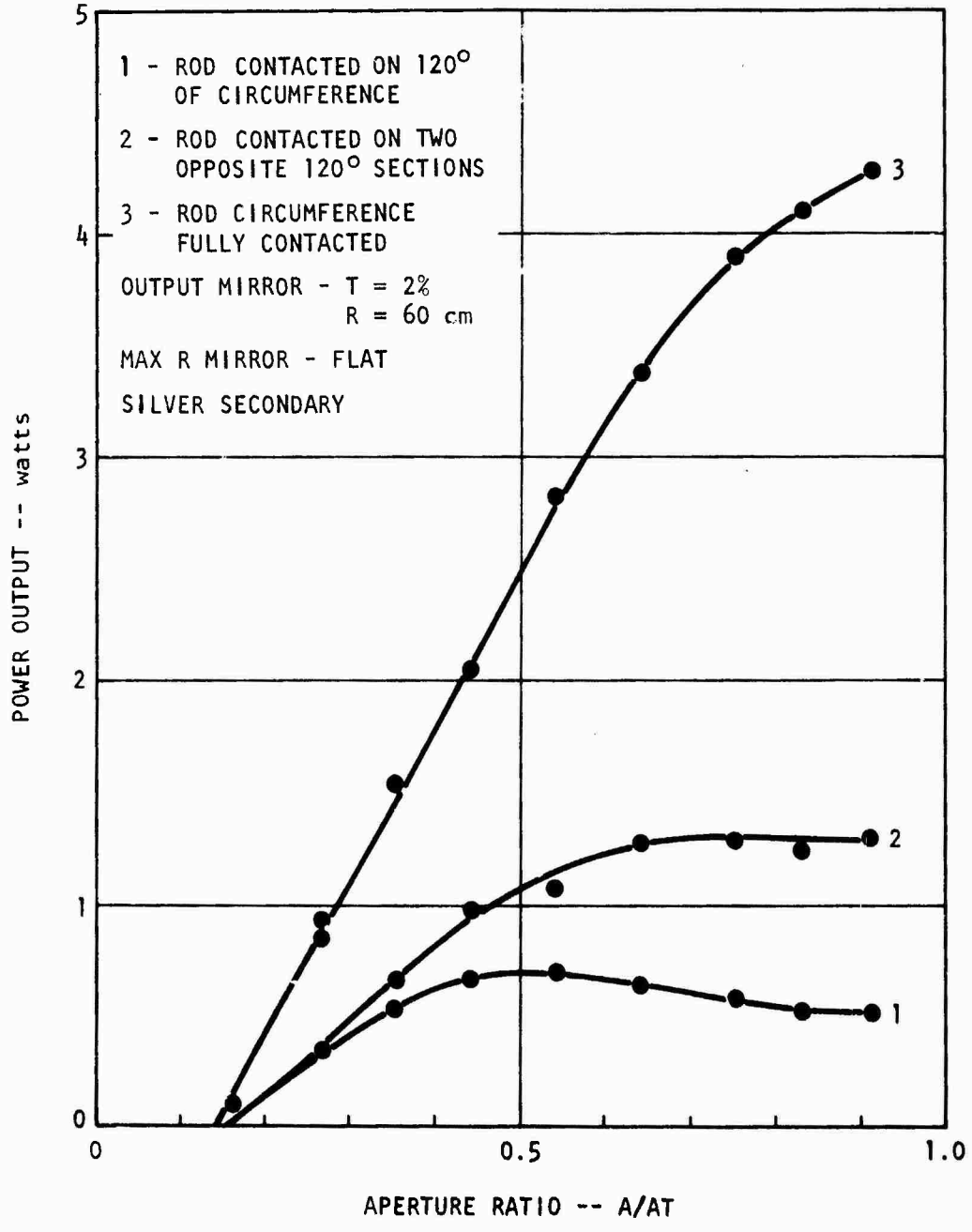

Figure 19 Sun Pumped Laser Performance With the Various Rod-Heat Sink Configurations

Section V

ANALYTICAL MODEL OF THE SUN PUMPED LASER

The multimode operation of the sun pumped laser at the earth's surface is depicted by the power output versus telescope aperture curves in Figure 18. It is of interest to project what the output of the laser would be outside the earth's atmosphere where the solar intensity is 1.6 times its value at the earth's surface. This is an important quantity since the application for the laser is the transmitter in a space optical communication system. Since the slope efficiency of the curves in Figure 18 decreases as the aperture ratio, A/AT, increases, it is not immediately obvious how to make this projection. We noted in Section IV that this behavior is due to the decrease in the transfer efficiency of the optical system as A/AT increases. The decreasing efficiency of the optical system with increase in A/AT was illustrated in Figure 4 and is due mainly to losses in the condensing cone. One might also suspect that the increasing heat load on the rod contributes to the effect, especially in view of the performance of the other heat sink configurations. However, it was verified that the decreasing efficiency of the optical system is primarily responsible for this behavior by determining the performance of the laser for both radial and sectorial variation of the telescope aperture (sectorial variation is enlarging a wedge shaped opening in the aperture). Figure 20 shows the variation of the laser output power with aperture for these two cases. The rod heat sink cap temperature was held constant at $50^{\circ}F$ for all values of A/AT. The pump power input to the laser rod varies linearly with sectorial increase of the telescope aperture, since there is no angular variation of the transfer efficiency. This is true because of the circular symmetry of the optical system. If the increasing heat load on the laser rod limits the performance of the laser, the slope efficiency should decrease with sectorial increase of the aperture as well as with radial increase. On the other hand, if these thermal effects are absent, the power output versus aperture for sectorial variation should be essentially a straight line. The latter is the case as seen in Figure 20, and we conclude that the multimode performance of this rod-heat sink configuration is not limited by the increasing heat load on the rod.

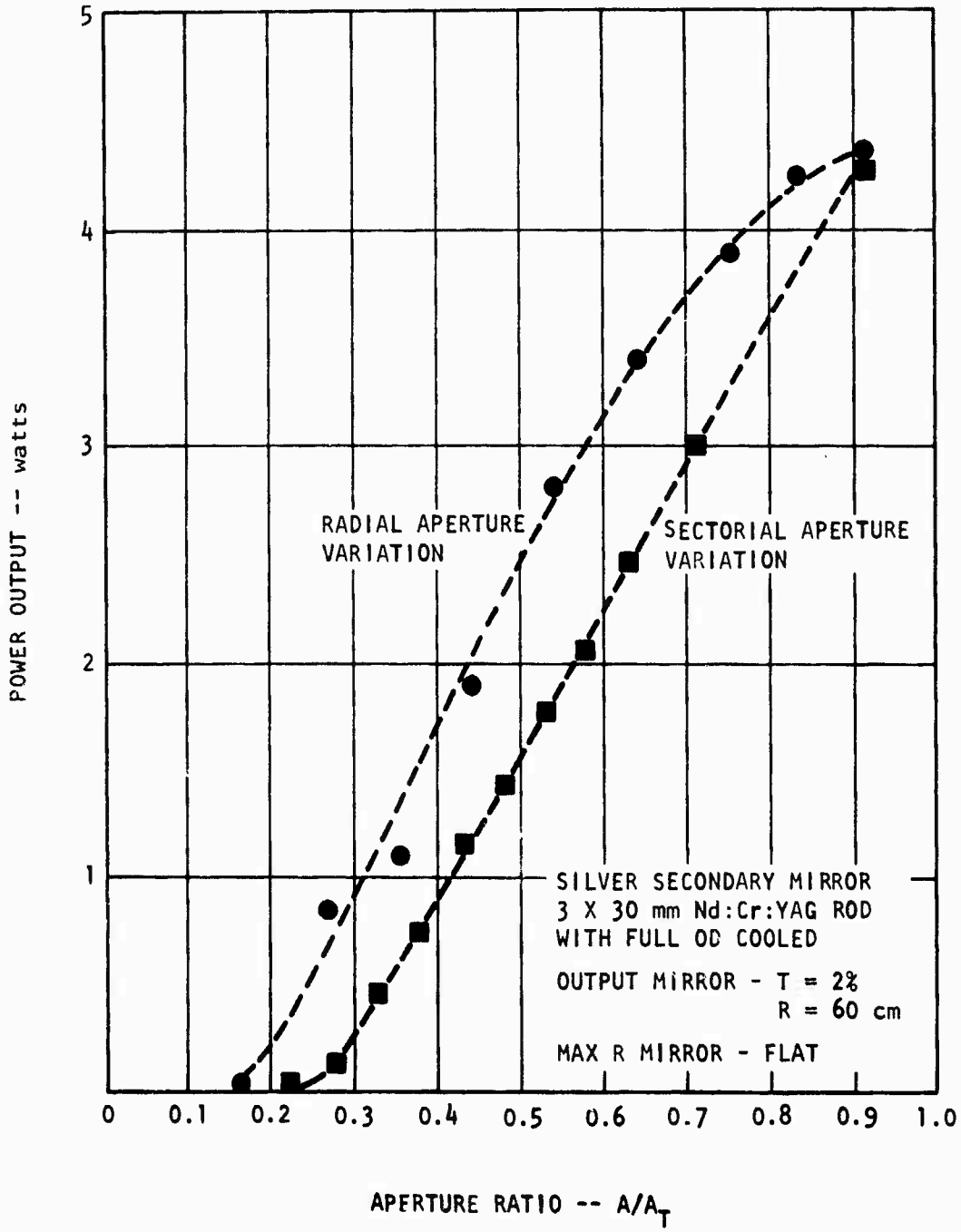

Figure 20 Sun Pumped Laser Output Power Variation With Radial and Sectorial Variation of the Telescope Aperture

The transfer efficiency of the optical system decreases with increasing mirror diameter because the light rays are incident on the coated optical elements at steeper angles (AR coatings less efficient) and make more reflective bounces traversing the condensing cone. We can obtain a quantitative estimate of this decrease in transfer efficiency by applying an analytical model of the cw YAG laser to the sun pumped laser results. From this analysis it will also be clear how to properly project the laser output power for solar radiation outside the earth's atmosphere.

The output power of the cw YAG laser is related to the laser's small signal gain by the formula[4]

$$P_{out} = \frac{T}{\beta} \left(\frac{g_o}{\alpha} - 1 \right) \tag{1}$$

where $\alpha = T/2 + \alpha_o$

T = total transmission of both laser mirrors

α_o = single pass dissipative loss

β = gain saturation parameter

g_o = small signal gain

The small signal gain is related to the power input to the pump lamp by

$$g_o = K(P_{in} - P_o) \tag{2}$$

For the lamp pumped case the proportionality factor is given by

$$K_{SP} = \frac{1}{d} \left(\frac{\beta A}{2} \right) \left(\frac{N_1 \sigma_p \eta}{2} \right) \left(\frac{\lambda P}{\lambda L} \right) k_p k_r \tag{3}$$

where d = laser rod diameter

A = laser rod cross sectional area

N_1 = ground state laser ion density

σ_p = average pump light absorption cross section

η = quantum efficiency of laser material

λ_p = average pump light wavelength

λ_L = laser wavelength

k_p = pump cavity efficiency

k_r = lamp radiant efficiency

The quantity P_o is the lamp threshold power. For end pumping of the laser rod the K factor is given by

$$K_{EP} = \left(\frac{\beta\eta}{4}\right)\left(\frac{\lambda p}{\lambda_L}\right) \quad k_p k_r \tag{4}$$

with the assumption that the rod length is longer than the 1/e pump light attenuation length of the crystal. From Figure 11 it is observed that this is indeed the case here.

For the case of the sun pumped YAG laser the radiant efficiency factor, k_r, does not apply, $P_o = 0$, and the factor, k_p, may be interpreted as the transfer efficiency of the optical system. Furthermore, the quantity P_{in} now corresponds to the sunlight power incident on the telescope mirror. The output power from the sun pumped laser may then be written

$$P_{out} = \frac{T}{\beta}\left(\frac{KP_{in}}{\alpha} - 1\right) \tag{5}$$

or

$$P_{out} = \frac{KP_s T}{\alpha\beta}\left(A - \frac{\alpha}{KP_s}\right) \tag{6}$$

where P_s = power density of radiation incident on the telescope mirror

A = area of mirror or of the exposed telescope aperture

Let us normalize the aperture area, A, to the total aperture area available, A_T, with the 24" diameter telescope; we then have

$$P_{out} = \frac{KA_T P_S T}{\alpha\beta}\left(\frac{A}{A_T} - \frac{\alpha}{KA_T P_S}\right) \tag{7}$$

The transfer efficiency of the optical system, k_p, may be expressed as

$$k_p = k_o k_T(d) \tag{8}$$

where k_o is the transfer efficiency in the limit of zero mirror diameter, d. The factor $k_T(d)$ varies from one to some number between zero and one as d varies from zero to D_M, the maximum telescope aperture diameter (24 inches in this case). Equation (6) may then be written

$$P_{out} = \frac{K'A_T P_s k_o k_T T}{\alpha\beta}\left(\frac{A}{A_T} - \frac{\alpha}{K'A_T P_s k_o k_T}\right) \tag{9}$$

where $$K' = \left(\frac{\beta\eta}{4}\right)\left(\frac{\lambda p}{\lambda_L}\right)$$

Let $K^* = K'A_T P_s k_o$, equation (8) then becomes

$$P_{out} = \frac{K^* k_T T}{\alpha\beta}\left(\frac{A}{A_T} - \frac{\alpha}{K^* k_T}\right) \tag{10}$$

Let us assume that the variation of the optical system transfer efficiency may be approximated by the form

$$k_T = 1 - a\,d^2 \tag{11}$$

where d is the nomalized telescope aperture diameter

$$d = \frac{d_{apert}}{D_m} \tag{12}$$

We have obtained a close fit of equation (10) to the experimental data in Figure 20 using a value of a = 0.4 in equation (11). The quantities α/K^* and $K^*T/\alpha\beta$ are first determined from a straight line fit to the P_{out} vs A/A_T curve in Figure 20, using a value of $k_T = 0.6$. This value of k_T is obtained by setting d = 1 in equation (11). The quantities so obtained are

$$\frac{\alpha}{K^*} = 0.162$$

$$\frac{K^*T}{\alpha\beta} = 11.3$$

Using these values of α/K^* and $K^*T/\alpha\beta$, the equations (10) and (11) are then used to calculate the theoretical P_{out} vs A/A_T curve for radial variation of the aperture. The central obscuration of the 7 inch diameter secondary mirror mount was accounted for in these calculations. With this obscuration

$$A/A_T = d^2 - (7/24)^2 \tag{13}$$

The results of these calculations are shown by the theoretical curves in Figure 21. A close fit to the experimental date points was obtained indicating that the model provides a fairly accurate description of how the transfer efficiency varies with telescope aperture or mirror diamater. With the value of a = 0.4 in equation (11) used to generate the radial variation curve, we find that the transfer efficiency decreases 40% as the telescope aperture is increased to 24 inches. This result suggests that considerable improvement in the laser performance could be realized with a more efficient relay system design.

The laser output power which would be obtained outside the earth's atmosphere can be calculated using equation (9). The value of P_S outside the

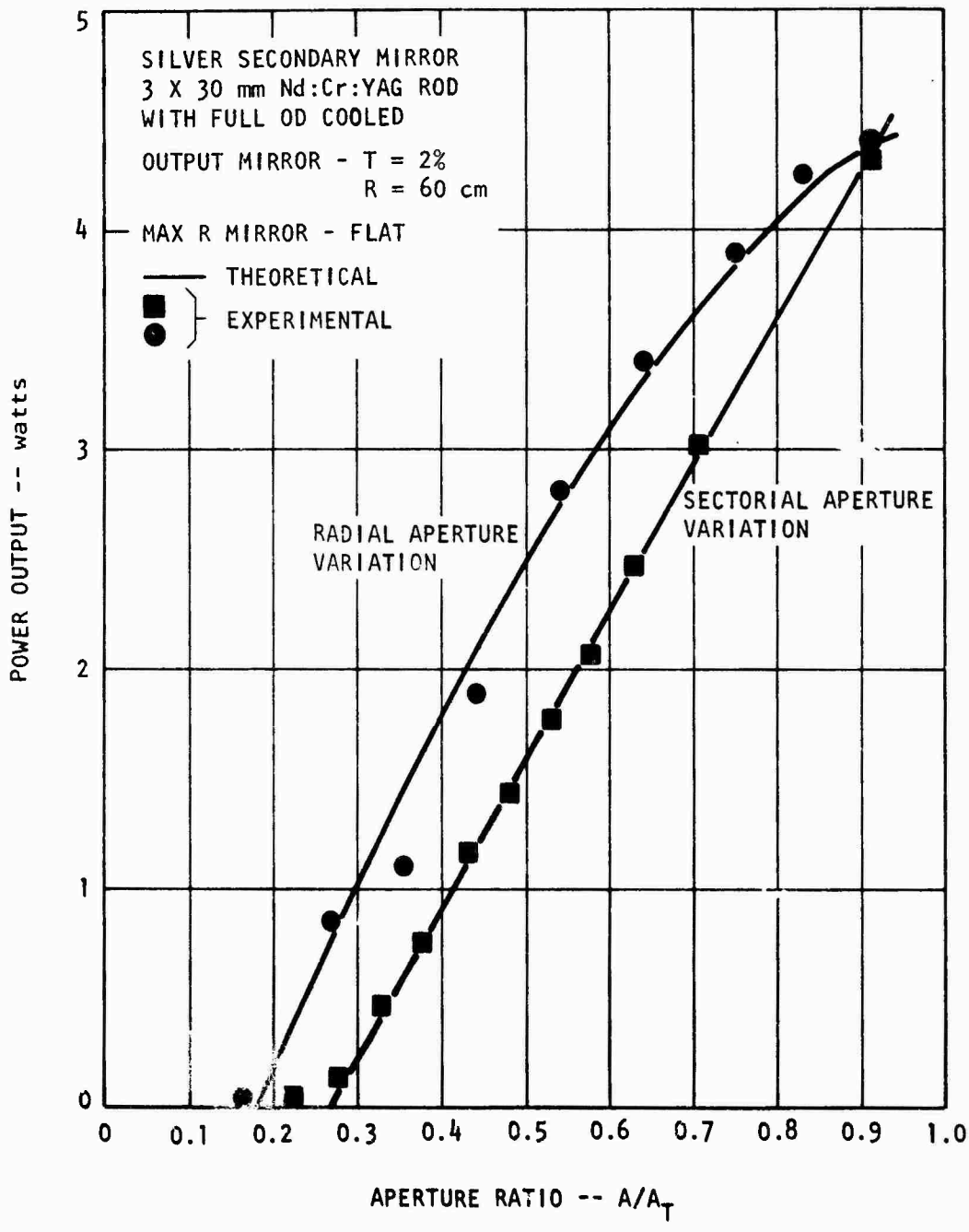

Figure 21 Theoretical Fit of Analytical Model to the Laser Performance

earth's atmosphere is 1.6 times its value at the earth's surface (see Table III). We will make the assumption that the power in the pump band regions is increased by the same factor on the average. The exospheric laser output power is thus calculated using the values

$$\frac{\alpha}{K^*} = .102$$

$$\frac{K^*T}{\alpha\beta} = 18.0$$

This calculation has been made as a function of mirror diameter and the results are shown in Figure 22. The same optical transfer efficiency relation and central obscuration were used to obtain the curves in Figures 21 and 22. Note that this procedure for calculating the laser power outside the earth's atmosphere for a 24 inch diameter mirror is equivalent to extending the sectorial variation curve in Figure 21 and reading the power output corresponding to an A/A_T value of (1.6) (.915).

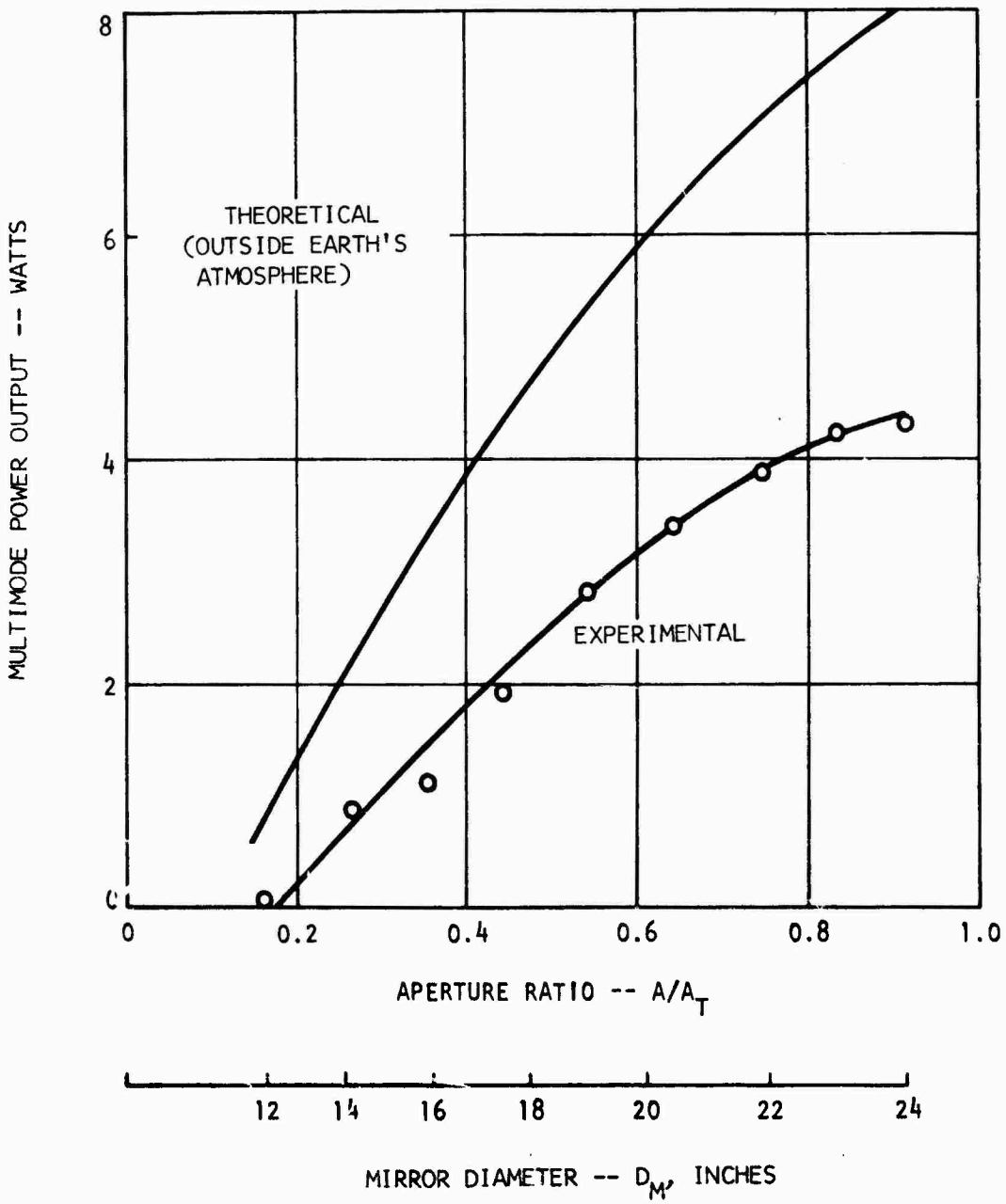

Figure 22 Predicted Performance of the Laser Outside the Earth's Atmosphere Compared with Experimentally Measured Performance on Earth

Section VI

FUNDAMENTAL MODE OPERATION

1. RESONATOR CONFIGURATION

Fundamental mode operation of the laser transmitter in an optical communication system is required for a number of reasons. The small divergence of the nearly diffraction limited beam permits use of smaller transmission and collection optics. The beam may be focused to a smaller spot in the modulating crystal permitting greater modulation depths to be obtained. Shorter pulses with greater pulse to pulse amplitude stability can be obtained from a TEM_{oo} mode locked laser. Finally, TEM_{oo} mode operation is required in a single frequency system with respect to modulation and demodulation of the carrier as well as obtaining single frequency operation of the laser.

The Nd:YAG laser normally oscillates simultaneously in many transverse spatial modes. The laser may be made to produce an output which consists of a single transverse mode, the fundamental or gaussian mode, by introducing into the resonator a selective loss which allows the TEM_{oo} mode to oscillate but prevents higher modes from oscillating. Since the diameters of the higher order modes are larger than that of the fundamental mode, this may be accomplished using an aperture stop of the appropriate diameter.

Efficient conversion from multimode to fundamental mode operation of the laser requires that the diameter of the TEM_{oo} mode be large enough to make efficient use of the pumped volume of the rod. For typical laser resonators of physically compact design this diameter is usually quite small. Consider, for example a laser resonator consisting of two mirrors with radii of curvature R_1 and R_2 separated by a distance d. The radius of the fundamental mode at the position of the mirror with radius of curvature R_1 is given by[5]

$$w_1^4 = \left(\frac{\lambda R_1}{\pi}\right)^2 \frac{R_2 - d}{R_1 - d} \frac{d}{R_1 + R_2 - d} \qquad (1)$$

The quantity w is the radius at which the beam power density has dropped to $1/e^2$ of its on axis value. The beam waist lies somewhere between the two mirrors and the maximum mode diameter is at the mirror position the farthest from the beam waist. For optimum TEM_{oo} mode operation the laser rod would be positioned near this mirror. Using equation (1) the maximum mode diamter, $2w_1$, for a resonator with R_1 = 60 cm, d = 25 cm and $R_2 = \infty$ is calculated to be $2w_1$ = 0.8 mm. This resonator configuration is not expected to result in efficient fundamental mode operation with a laser rod of 3 mm diameter since less than 1/9 of the rod volume is filled by the Gaussian mode. A common method of expanding the TEM_{oo} beam volume within the laser rod is to use longer radius mirrors with greater separation. For example, a beam diameter of 1.5 mm can be achieved with, R_1 = 100 cm, $R_2 = \infty$ and d = 75 cm. There are two disadvantages to using this approach for the communication laser application, however. First, the use of long radius mirrors with large mirror separation usually results in unstable operation due to alignment instabilities and optical perturbations within the laser rod. Stable operation is required for the communication laser. Secondly, the resonator length in a mode locked laser communication system is constrained by the data rate requirements of the system. For a data rate of 500 bps and a rod length of 30 mm the resonator length required is 27.4 cm.

An alternate approach to expanding the diameter of the fundamental mode within the laser rod is the use of an intracavity lens.[6,7,8] Large fundamental mode diameters can be achieved with this scheme without the use of long radius mirrors and large mirror separations. A resonator configuration using an intracavity lens is shown in Figure 23. The diameter of the fundamental mode may be calculated at every axial position within this resonator with the use of ray transfer matrix theory.[5] Any laser resonator may be represented by an equivalent periodic sequence of optical elements. The ray transfer matrix relates the parameters of the beam (the beam radius and radius of curvature) at one axial position in this sequence to those at another. The beam radius, w, and radius of curvature, R, are related to the

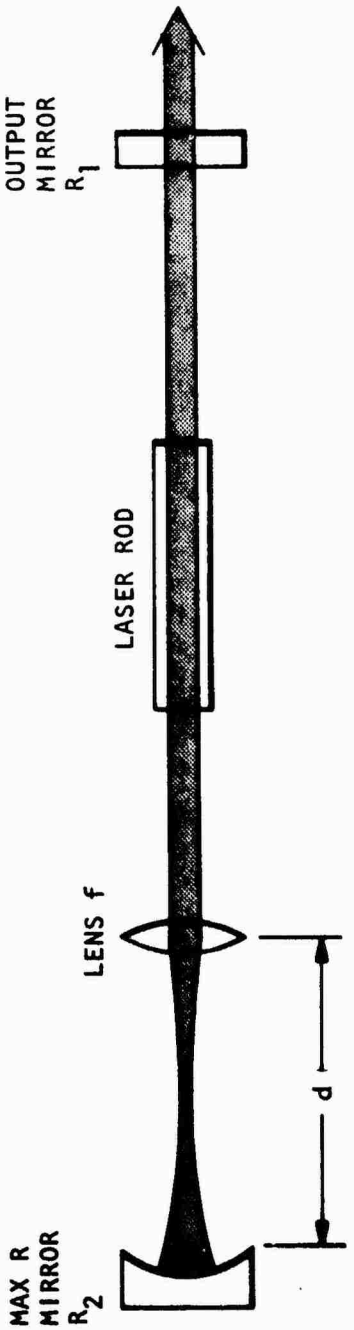

Figure 23 Resonator Design Using an Intracavity Lens

complex beam parameter, q, by

$$\frac{1}{q} = \frac{1}{R} - i\frac{\lambda}{\pi w^2} \tag{2}$$

The beam parameters q_1 and q_2 at two axial positions in the sequence are related by

$$q_2 = \frac{Aq_1 + B}{Cq_1 + D} \tag{3}$$

where A, B, C and D are the elements of the transfex matrix. If the distance between positions 1 and 2 is equivalent to one round trip through the resonator, we must have $q_1 = q_2$ since the properties of the beam must remain the same after one round trip through a stable resonator. This condition results in a quadratic equation in q which may be solved to yield

$$\frac{1}{q} = \frac{D-A}{2B} \mp \frac{i}{2B}\sqrt{4 - (A+D)^2} \tag{4}$$

$$R(Z) = \frac{2B}{D-A} \tag{5}$$

$$w^2(Z) = \left(\frac{2\lambda B}{\pi}\right) \Big/ \sqrt{f - (A+D)^2} \tag{6}$$

The beam diameter and radius of curvature at every point Z within the resonator may be calculated using equations (5) and (6). The reader is referred to reference (5) for the detailed development of equations (5) and (6). Also included in this reference are the ray transfer matrices for various optical elements.

We have used a computer program[9] to solve for the fundamental mode radius in the sun pumped laser using the above procedure. The resonator configuration is shown in Figure 24. The mode radius at either end of the laser

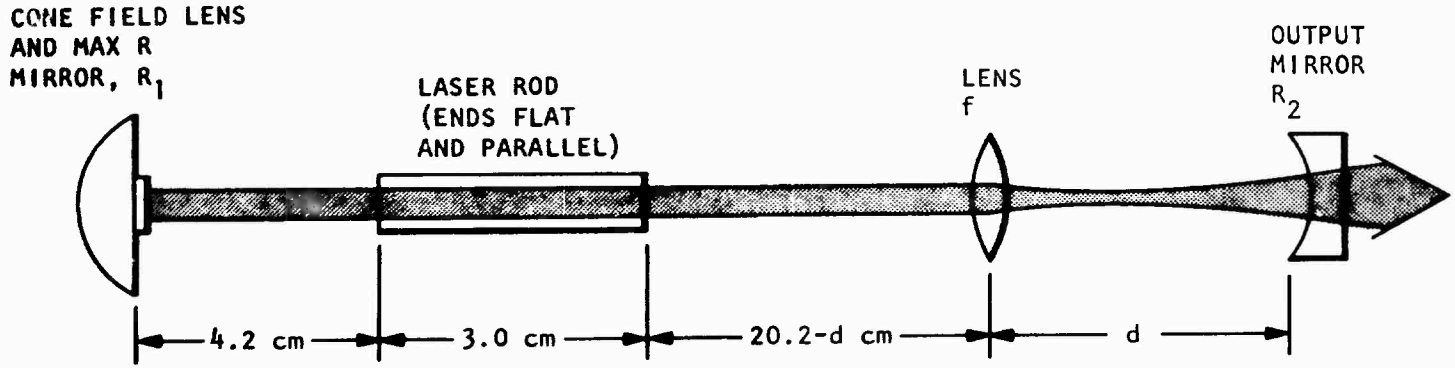

Figure 24 Sun Pumped Laser Resonator Configuration

rod and in the middle of the rod and the mode volume within the rod were calculated for various values of R_1, R_2 and d. The results of these calculations are shown in Figures 25, 26 and 27. The mode radius plotted in these graphs is the radius in the middle of the rod; it was found that for mode diameters of interest the mode is well collimated within the rod. It is observed from the graphs that for each value of R_1, there is a minimum separation of the lens-mirror combination and a maximum separation at which the mode radius becomes very large. Outside of these minimum and maximum values of d the resonator is not stable, and laser oscillation cannot be sustained. A given mode radius can thus be obtained at two values of d. We have found, however, that more stable operation of the laser is obtained with the smaller value of d; this observation is in agreement with the results of the computer program which also calculates the sensitivity of the resonator to mirror misalignment. The lower stability limit of d is seen to be slightly smaller than the lens focal length for the flat mirror and slightly greater for the convex mirror. A comparison of how the mode radius varies with d for the case $R_2 = 5$ cm is shown in Figure 27. The radius minima occur at different values of d, but the values of the minima and the range of d for stability are approximately the same for both the flat and convex mirrors. Fundamental mode operation is therefore expected to be similar for the two mirrors; operation is reportedly more stable, however, using the convex mirror.[7]

A given mode radius may be obtained with any value of R_2 greater than some minimum value by proper choice of d. For example, Figures 25 and 26 show that a mode radius of 0.81 mm is obtained with 1 cm $< R_2 < \infty$. For any given mode radius, however, the required value of d is farther from the stability limits if the mode radius is close to the minimum radius. This implies that better TEM_{oo} mode operation will be obtained with the shorter radius concave mirrors; we have observed this effect experimentally with the operation of the sun pumped laser. There is, of course, a lower limit to R_2 below which TEM_{oo} performance will decline. If the mode radius becomes too large, the optical loss due to the aperturing of the laser rod will begin to limit the TEM_{oo} output.[7]

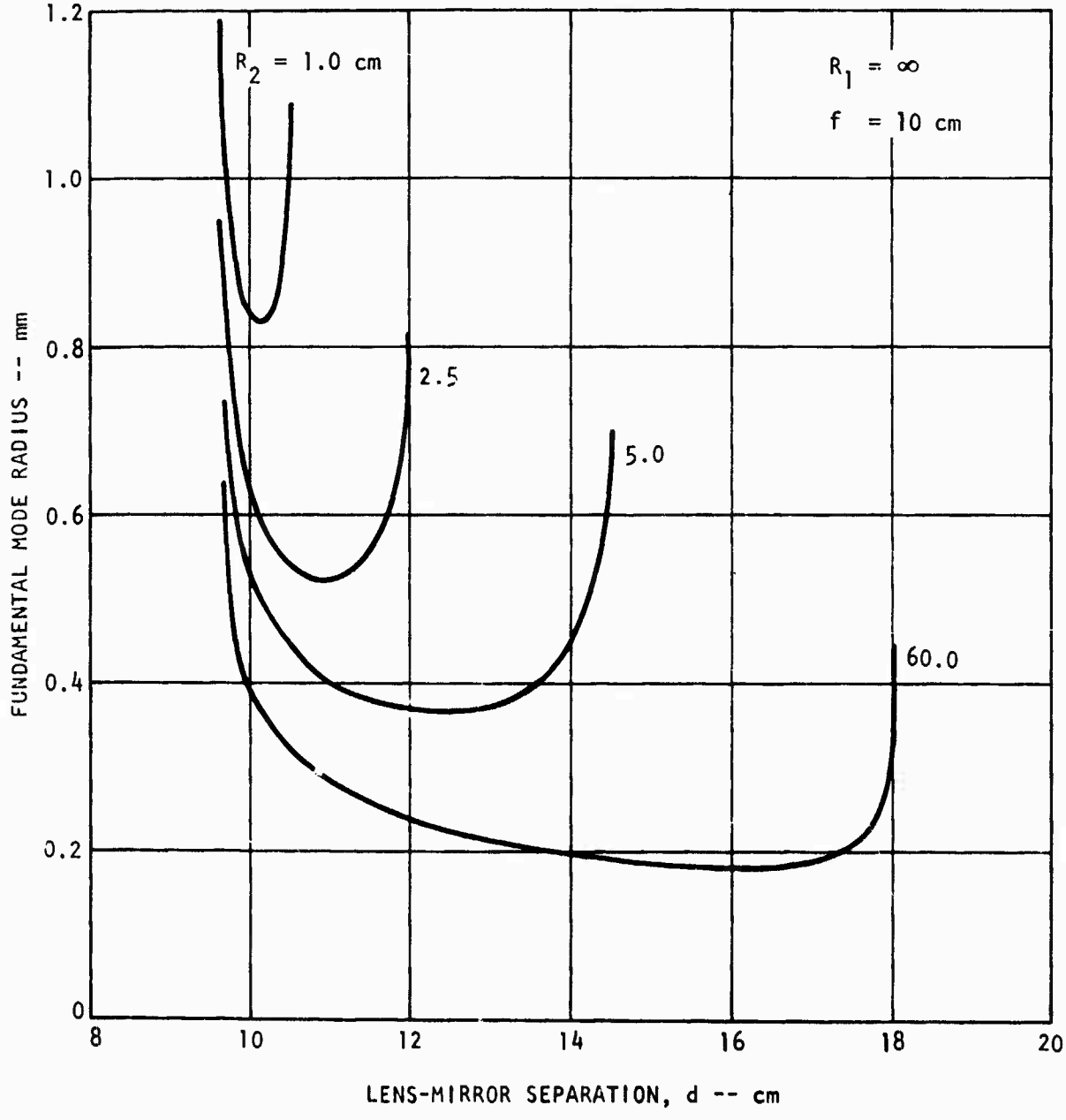

Figure 25 Mode Radius Versus Lens-Mirror Separation With Flat Rear Mirror

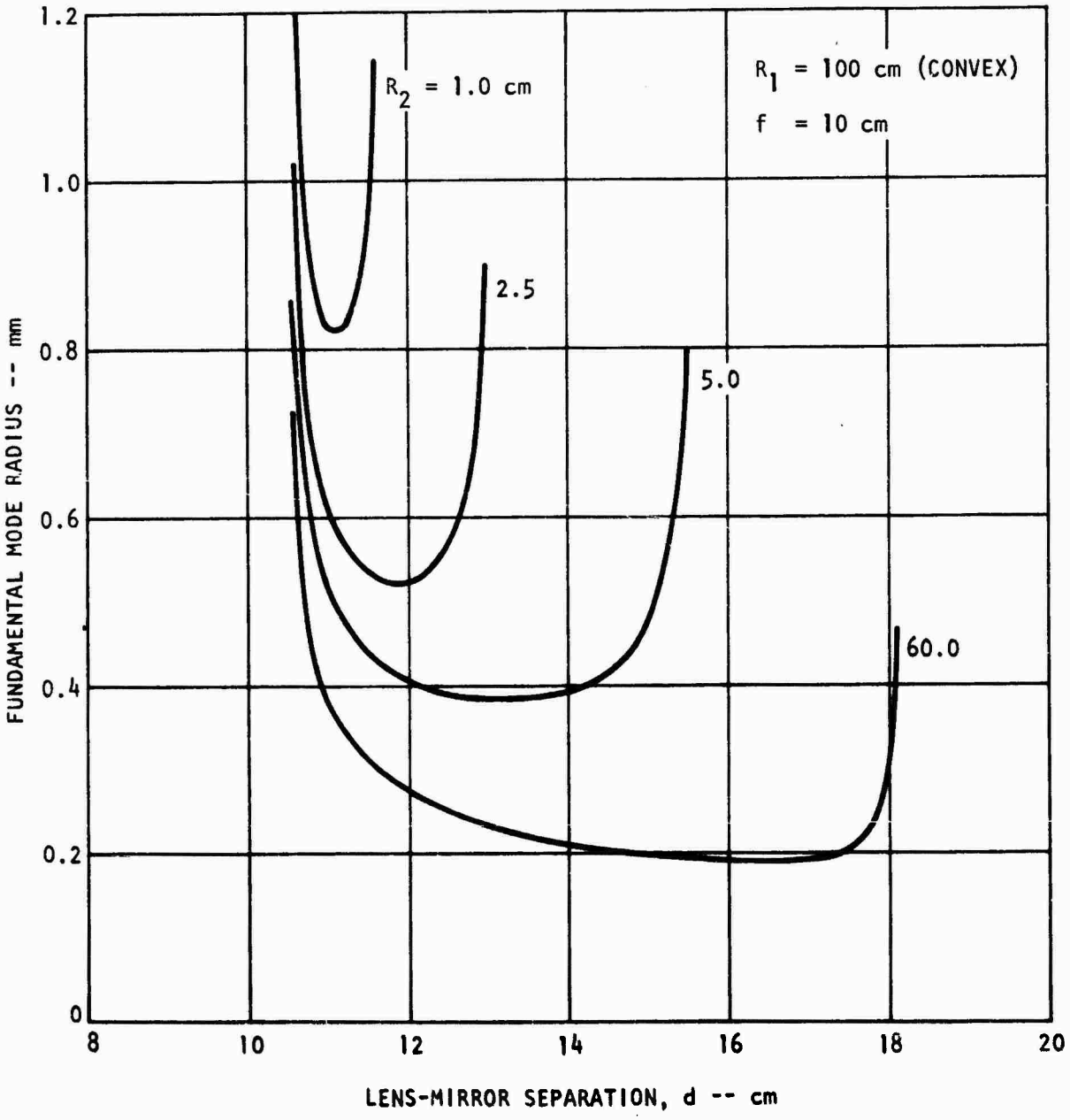

Figure 26 Mode Radius Versus Lens-Mirror Separation With Convex Rear Mirror

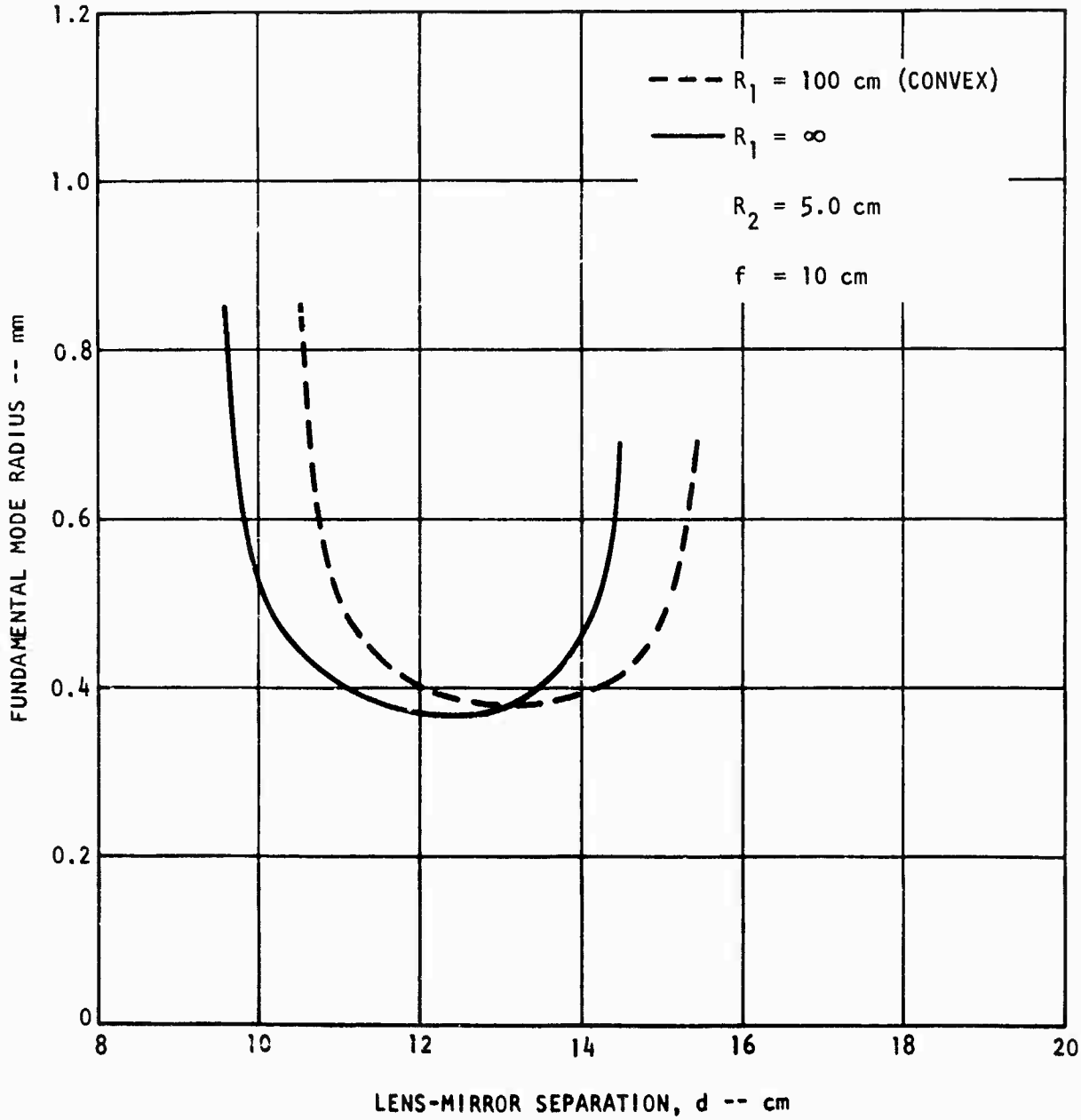

Figure 27 Comparative Variation of Mode Radius for Flat and Convex Rear Mirrors

The choice of the focal length of the intracavity lens is based primarily on physical dimensional considerations. The resonator length is fixed by the data rate requirement, 500 MHz in this case. The position of the lens within the resonator is limited by mechanical design parameters and the requirement for space to insert the mode locking modulator near the output mirror. For our case here, a convenient focal length was 10 cm. With this short lens focal length, the thermal lensing in the rod is a small perturbation, having little effect on the mode diameter. For the above calculations, a rod focal length of 250 cm was used.

2. EXPERIMENTAL RESULTS

The resonator configuration shown in Figure 24 was used to obtain fundamental mode operation of the sun pumped laser. The experimental apparatus is shown in Figure 28. Both the intracavity lens and the mode locking modulator are shown mounted in the resonator in this photograph. The laser output power was measured using a CRL model 212 power meter. A portion of the output beam was split off and directed to a Hewlett-Packard model 4205 photodiode. The output of the photodiode was displayed on either a spectrum analyzer or a sampling oscilloscope.

Using the laser rod-heat sink configuration shown in Figure 14b, and the 3 x 30 mm Nd:Cr:YAG rod a TEM_{oo} mode output power of 0.6 watts was obtained (mode locking modulator not in resonator). This performance was obtained with the silver secondary mirror and the full 24 inch telescope aperture opened. The resonator mirror radii were $R_1 = \infty$ and $R_2 = 5$ cm and the output mirror transmission was 2%. Fundamental mode operation was obtained by adjusting the spacing between the lens and the output mirror. An intracavity aperture was not necessary; the aperture of the laser rod itself was sufficient to surpress the higher order modes. The output beam was observed visually using a Kodak infrared viewing card. It was noted that visual observation of the beam pattern alone was not sufficient to determine the existance of TEM_{oo} mode operation. Examination of the frequency spectrum of the laser output showed that other modes in addition to the fundamental mode may be oscillating even though the beam pattern appears visually uniform. Figure 29a shows the frequency spectrum of the laser output with the laser operating predominantly

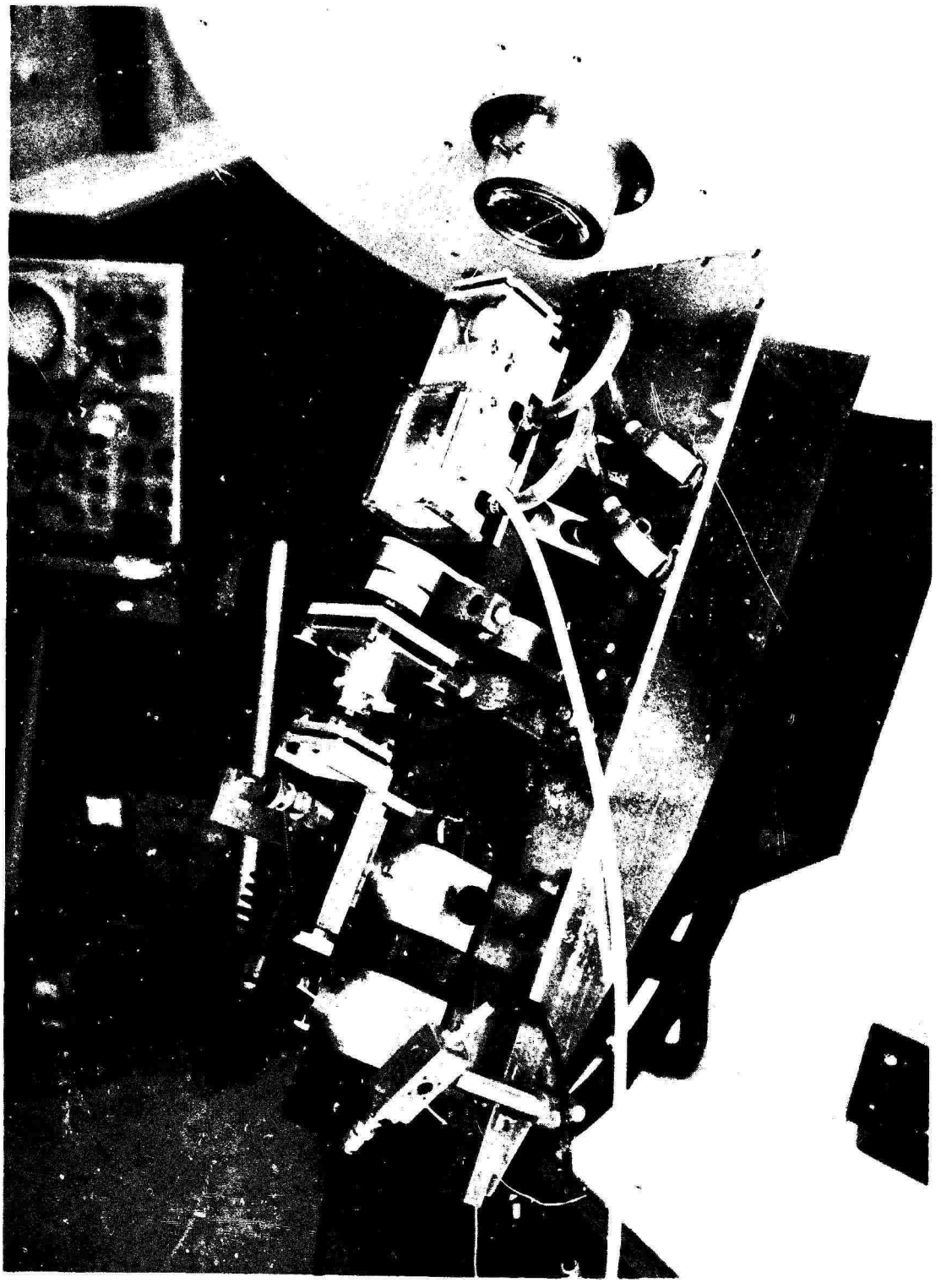

Figure 28. Sun Pumped Laser Apparatus

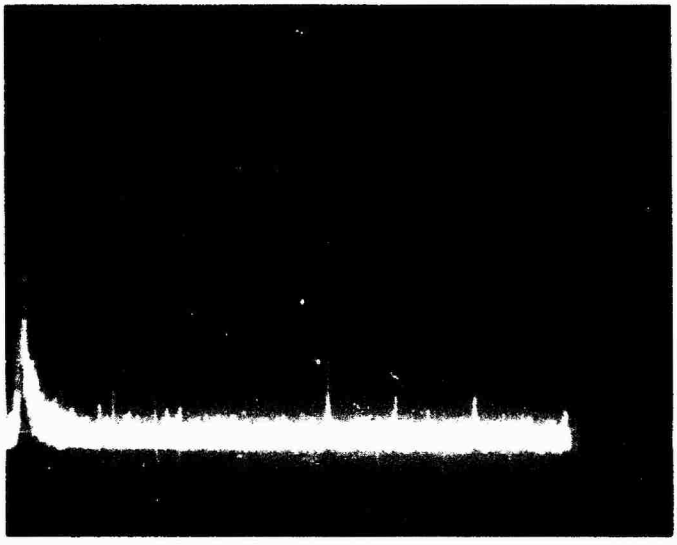

a.

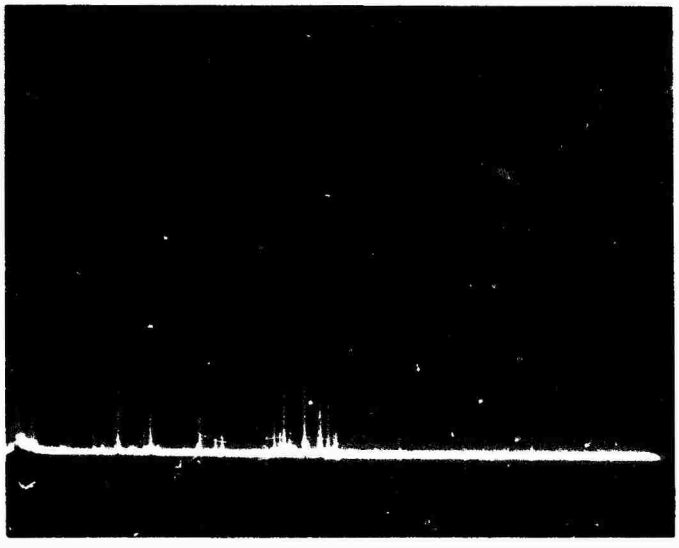

b.

Figure 29 Frequency Spectra of the Sun Pumped Laser Output, 100 MHz Per Divisions (a. - laser operating in TEM_{00} mode, b. - laser operating multimode) **The zero frequency marker is at the extreme left of the photograph.**

in the fundamental mode; only the fundamental C/2L beat frequency at about 500 MHz is present. Figure 29b shows a typical frequency spectrum with the laser operating multimode. The additional frequencies in this display are generated by the beating between the many transverse modes. A Tektronix 531A oscilloscope with an NR spectrum analyzer plug-in unit was used to obtain these frequency spectra. In general, it was found that as the lens-mirror separation d was decreased from the point where the beam pattern first became visually uniform to the point where essentially spectrally pure TEM_{oo} mode operation was obtained, the laser output power dropped about 20%. Thus, visual inspection of the beam pattern alone over-estimated the TEM_{oo} mode power by about 20%.

The TEM_{oo} mode performance of the laser was observed using output mirrors with radii of curvature of 5 cm, 60 cm and 7 m, all with 2% transmission. The highest fundamental mode output was obtained with the 5 cm radius mirror in agreement with the predictions of the computer study. The laser was also operated with a convex maximum reflectivity mirror with a radius R_1 = 50 cm. The behavior of the laser with this mirror was about the same as with the flat mirror, although the stability of operation with the convex mirror was not accurately recorded. We, therefore, annot conclude whether the stability behavior of the resonator with the convex and flat mirrors is in agreement with the predictions in reference (7).

One disadvantage of the intracavity lens resonator configuration is the insertion loss of the lens. Even the fractional percentage dissipative loss of such an element can result in significant reduction of the output power of the low gain laser. With the laser operating multimode at a power output of about 4 watts, insertion of the lens was observed to reduce the laser output about 25%. To make this determination, the lens was positioned to yield the maximum multimode output power. Some of this power reduction may be attributable to reduction in the mode order with insertion of the lens, even so adjusted. It is likely, however, that most of the loss is due to reflection and scattering losses at the lens surfaces, even though the lens was antireflection coated for nominally less than 0.1% reflectivity per surface. Considerable improvement in the TEM_{oo} mode performance of the laser could be realized by grinding the lens onto the end of the laser rod.

The TEM_{oo} mode performance cited above represents a conversion of only about 15% of the multimode output of the sun pumped laser to the fundamental mode. On the other hand, multimode to fundamental mode conversion efficiencies of 30-50% have been observed for conductively cooled, lamp pump lasers on the Space Laser Design project[3] using the same resonator configuration. There are four effects which are believed to be responsible for the difference in the TEM_{oo} performance of the two lasers. In order of decreasing importance, these effects are:

1. Large axial thermal gradient in the laser rod due to the end pumping geometry. Results in large transverse thermal gradients and high temperatures on the rod axis at the input end of the rod.
2. Larger heat load on the laser rod with chromium pump absorption than is obtained for lamp pumped laser with Nd only doped rod. Results in larger transverse thermal gradients and on axis rod temperatures.
3. Possible non-uniformities in the contact of the rod to the heat sink and in the heat flow path from the rod to the cooling pipe, can result in rod thermal variations which cause optical distortion.
4. Stronger pumping of the edge of the laser rod in the end pumping geometry as compared to the focusing lamp pump cavity geometry. Results in relatively less gain on the axis of the rod which does not favor the gaussian TEM_{oo} mode.

The first two effects noted may likely be attenuated by reducing the rod doping concentrations without adversely affecting the multimode performance of the laser. This is evident from Figure 11, which shows that most of the pump light is absorbed in the first cm of the rod. The fourth effect, if real, is a property of the end pumping geometry, and there does not appear to be any way to substantially reduce it. The third effect is believed to have limited the TEM_{oo} mode performance cited above because of the heat sink geometry.

The laser rod was contacted by the heat sink on its full circumference by placing a cap over the rod and heat sink wedge (Figure 14b). It is possible that uniform thermal contact between the rod and the heat sink, with the indium solder, was not made because of the manner in which the cap and wedge joined. Furthermore, both the cap and wedge were slotted. Solder flow through these slots may have resulted in nonuniformities in the contact. To determine whether this heat sink configuration did limit the TEM_{oo} output of the laser, the laser was operated with a new heat sink diagrammed in Figure 30. No slots were cut into the heat sink and the split is along a diameter of the laser rod. With this design it was possible to obtain a uniform layer of solder around the rod. Good uniform thermal contact between the cap and the bottom part of the heat sink was ensured by solder joining these pieces at the split line.

The second Nd:Cr:YAG rod which was damaged in an earlier experiment was repaired and used to evaluate the performance of the laser with this new heat sink. The laser was operated under the same conditions as above: silver secondary mirror, full telescope mirror exposed, $R_1 = \infty$, $R_2 = 5$ cm, focal length of lens = 10 cm and an output mirror transmission of 2%. With the new heat sink a TEM_{oo} mode output of 0.8 watts was obtained, a 33% improvement over the previous performance. Frequency spectra of the laser output are shown in Figure 31. These spectra were recorded using a Hewlett-Packard 8551B spectrum analyzer (RF section) with an 851B display section. The first two orders of the C/2L beat frequency were recorded with this analyzer which had a wider bandwidth than the one previously used. In Figure 31(a) the amplitude scale is linear and in (b) the amplitude scale is logarithmic. Figure 31(b) shows that the higher order modes present in the laser output are about 20 db below the fundamental.

A beam scan of the laser output is shown in Figure 32. The scan was made by sweeping the beam passed a 25 micron diameter pinhole with a rotating mirror and recording the output of a solar cell placed behind the pinhole. The scan was made through the beam axis. The beam profile is seen to be essentially gaussian with a small degree of nonuniformity near the beam axis.

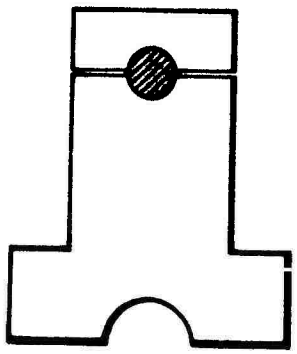

Figure 30 Cross Sectional View of Improved, Solid Copper Heat Sink

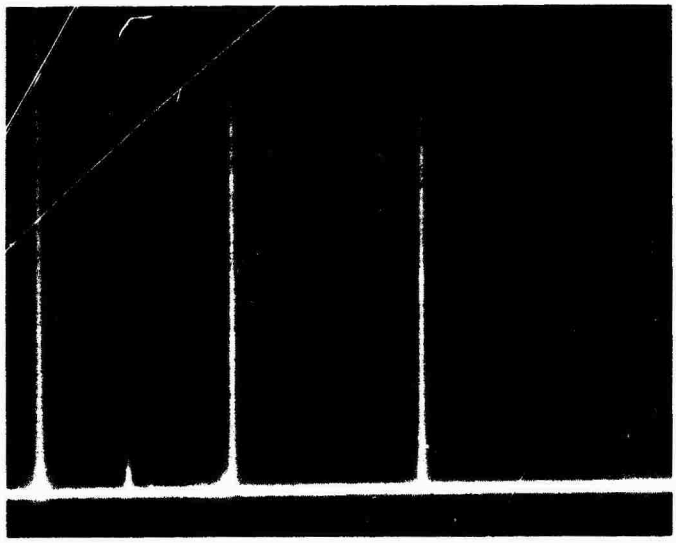

a.

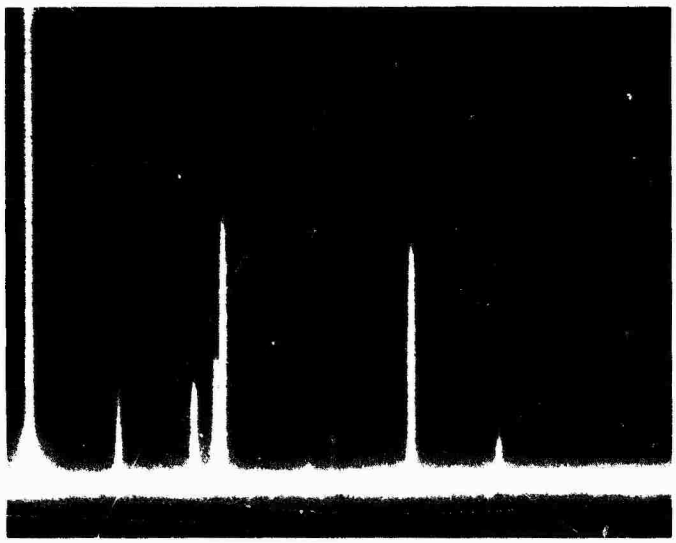

b.

Figure 31 Frequency Spectra of the Sun Pumped Laser Output, 200 MHz Per Division (a. - linear amplitude scale, b. - logarithmic amplitude scale) The zero frequency marker is at the extreme left of the photograph.

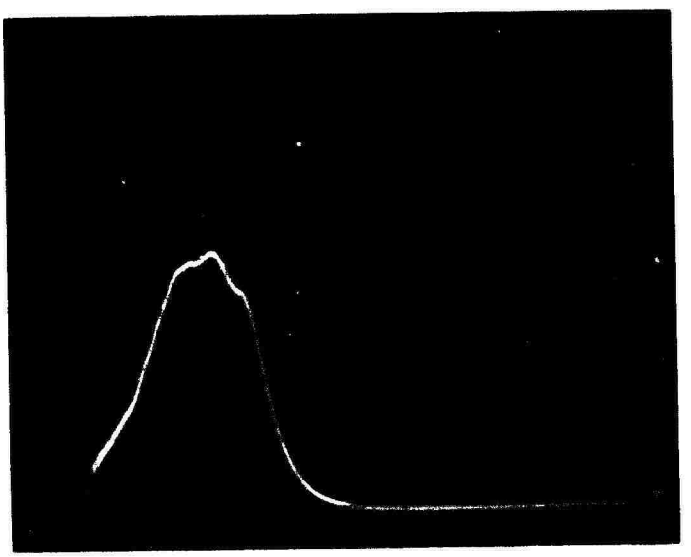

Figure 32 Measured Radial Variation of Beam Power Density

The time variation of the TEM_{oo} laser output was monitored by displaying the recorder output of the CRL model 212 power meter on a Tektronix 555 oscilloscope. The variation of the output power over a period of 20 seconds is shown in Figure 33(a). The noise on the laser output arises from an interesting source. In order to prevent moisture from condensing on the output end of the laser rod during operation, a plastic cover is placed over the laser head and dry nitrogen flowed into the head. The nitrogen exits through a hole in the cover through which the laser beam passes. The nitrogen flowing through the laser beam inside the resonator distorts the beam and causes the laser output to vary with time. This was verified by recording the laser output with various nitrogen flow rates. The results are shown in Figure 33(b), (c) and (d). The time variation, or instability of the laser output is due to the optical distortion caused by the nitrogen flowing through the laser beam path and is essentially eliminated by stopping the nitrogen flow.

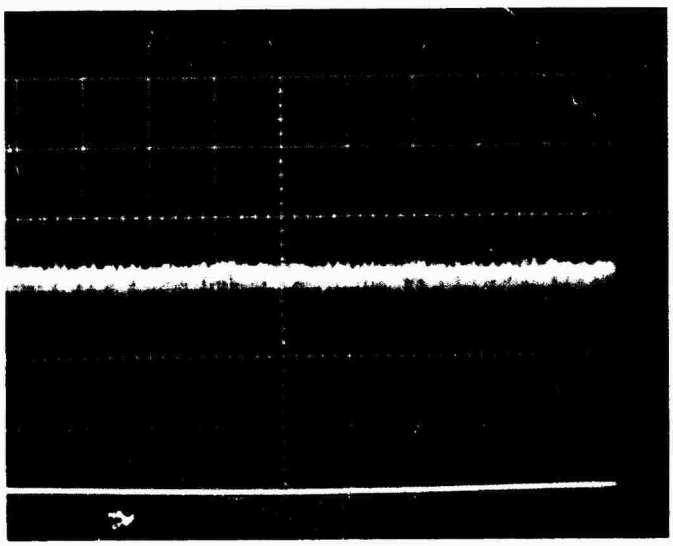

a.

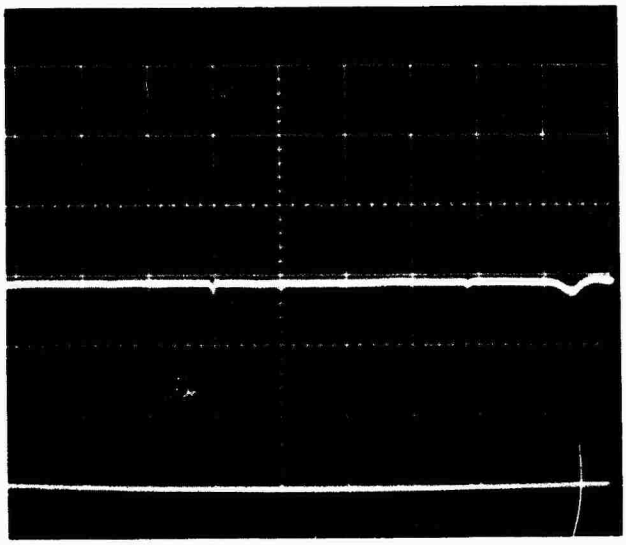

b.

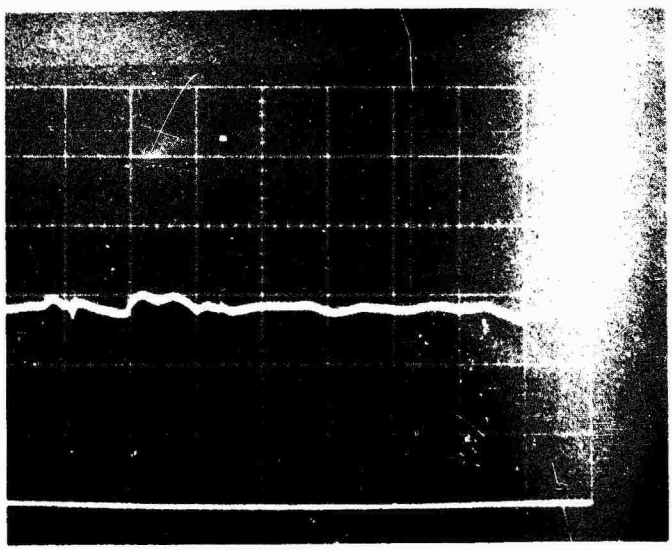

c.

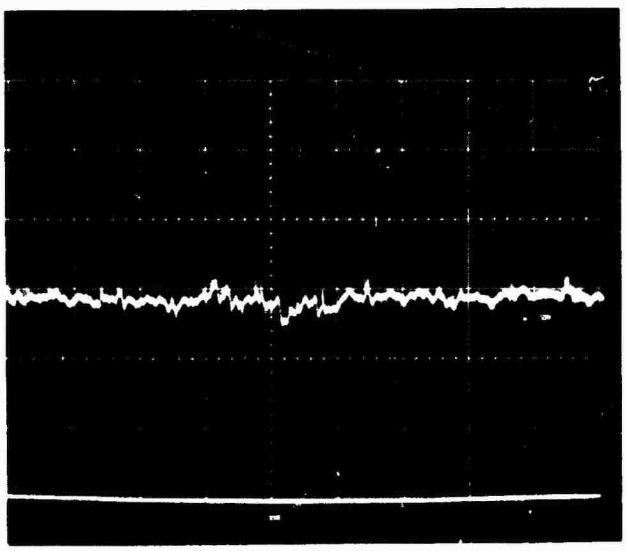

d.

Figure 33 Time Variation of the Sun Pumped Laser Output
(a. - time scale 2 sec/cm, low nitrogen flow rate;
b. - time scale 5 msec/cm, nitrogen flow stopped;
c. - time scale 5 msec/cm, low nitrogen flow rate;
d. - time scale 5 msec/cm, high nitrogen flow rate)

Section VII
MODE LOCKED LASER OPERATION

The sun pumped laser was mode locked using an intracavity phase modulator consisting of a 1 mm thick slab of $LiNbO_3$ placed in the resonator at Brewster's angle. A photograph of the modulator is shown in Figure 34. With the laser mode locked at approximately 500 MHz, a polarized output of 0.4 watts was obtained in the fundamental mode. The rod-heat sink assembly of Figure 13(b) was used for the mode locked laser experiment. The mode locked output of the laser, detected by the Hewlett-Packard 4205 photodiode, and displayed on a Tektronix 661 oscilloscope with a 4S2A sampling plug-in unit, is shown in Figure 35. The pulse length in this trace is limited by the rise time of the photodiode which is about 0.5 nsec. Stable mode locked operation of the laser could be sustained for a minute or two before readjustment of the modulator drive frequency was required. Pulse to pulse amplitude variation during this period was within $\pm$ 10%. An RF power of about 0.5 watts was required to drive the modulator.

The reduction in the TEM_{oo} mode output of the laser with the insertion of the Brewster angled modulator crystal is due primarily to the polarization of the laser. Insertion of a quartz Brewster plate into the resonator reduced the multimode output of the laser by 50%. The polarization loss was found to be very dependent in the polarization orientation, with the minimum loss occurring for the polarization vertical with respect to the rod heat sink. Thermal birefringence induced by absorption of the pump light is responsible for this polarization loss, which is higher than that observed for lamp pumped lasers. Over 80% of the unpolarized output from lamp pumped, conductively cooled lasers has been obtained polarized with the insertion of a quartz Brewster plate[3]. The first three effects discussed in Section VI, which are believed to limit the TEM_{oo} operation of the laser, probably also account for the high polarization loss.

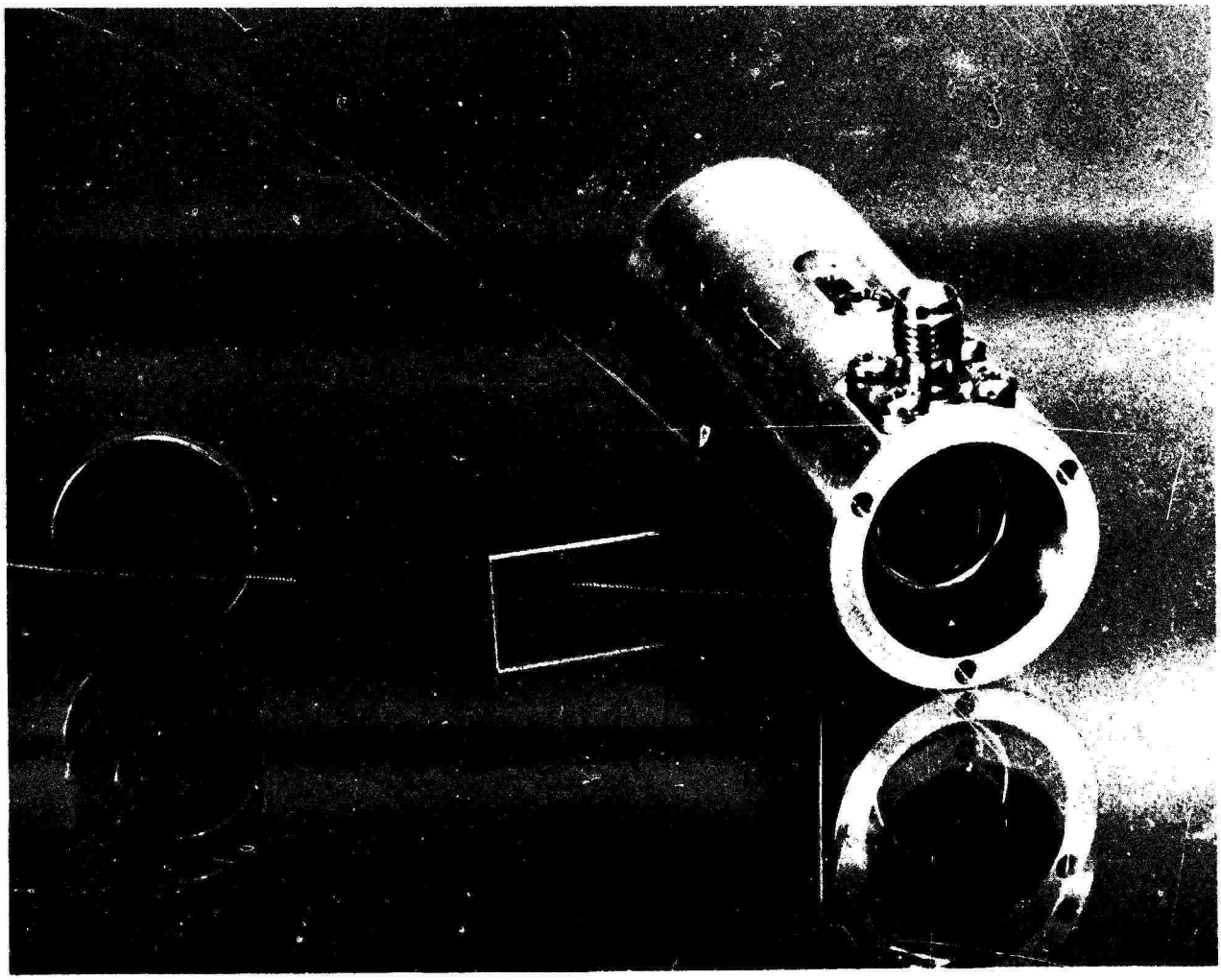

Figure 34 Mode-Locking Modulator

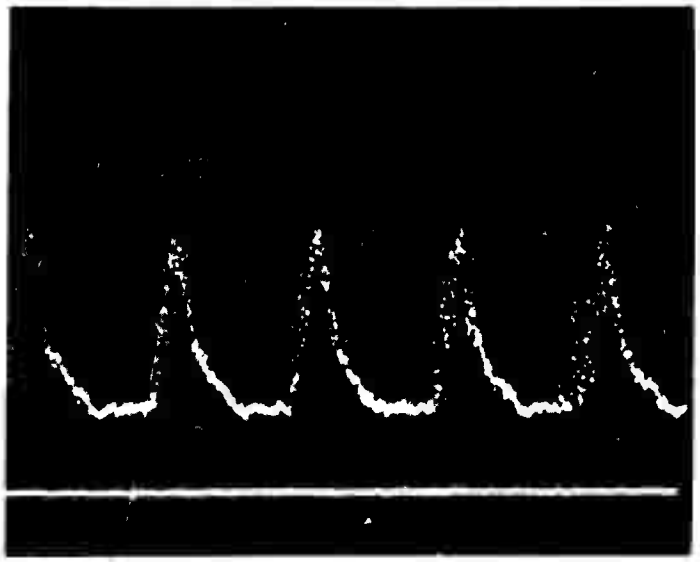

Figure 35 Temporal Output of the Mode Locked, Sun Pumped Laser (Time scale 1 nsec/cm)

Section VIII

SUMMARY AND CONCLUSIONS

Improved heat sinking of the laser rod on this contract resulted in an increase of multimode laser output power from 1.65 watts obtained on the previous contract to 4.85 watts. The results of the experiments showed that the lower operating temperature of the laser rod, obtained with the use of copper as the heat sink material, was more important to efficient laser operation than a good thermal expansion match between the rod and heat sink. Successful utilization of copper was possible because of the low yield strength of the indium solder used to bond the rod to the heat sink; the solder bond layer compensates for the thermal expansion mismatch between the rod and heat sink materials. Stress relief slots cut into the heat sink were found not to be necessary.

Experiments comparing the laser operation of various rod-heat sink configurations showed that adequate heat sinking of the laser rod was obtained only by fully contacting the circumference of the rod with the heat sink. A heat sink scheme with one third of the rod contacted by the heat sink, and two thirds of the rod circumference exposed to admit side pump light, was operated to show the dual pumping capability of the laser. The multimode performance of this configuration was considerably inferior to that later obtained with the rod fully contacted. Efficient sun pumped operation of the laser in a configuration compatible with side lamp pumping was, thus, not demonstrated. There are dual pumping schemes which do not have the disadvantages of the one tested here, however, and we do not conclude that dual sun and lamp pumping of the laser is not practical. Maximum performance of the laser in both operating modes, however, may require separation of these two functions. A system analysis is required to determine the optimum approach.

Operation of the sun pumped laser in the fundamental mode was obtained with the use of an intracavity lens to expand the mode size in the laser rod. The results of fundamental mode experiments are in agreement with the predictions of a computer analysis of the resonator. A TEM_{oo} mode output power

of 0.8 watts was obtained with the laser rod circumference fully contacted by the heat sink. This fundamental mode performance represents a multimode to TEM_{oo} mode conversion efficiency about one third of that being currently demonstrated by conductively cooled, lamp pumped lasers. The relatively poor fundamental mode performance of the sun pumped laser compared to that of the lamp pump laser is believed to be due primarily to the large axial thermal gradient in the laser rod resulting from the end pumping geometry. This axial gradient results in large transverse thermal gradients and a high on axis rod temperature at the input end of the laser rod. Lower rod doping concentration is suggested as a means of improving the TEM_{oo} mode performance of the laser. Further improvement in the laser operation could be achieved by grinding the intracavity lens onto the laser rod; the insertion loss of the lens reduced the multimode output of the laser by 25%.

Mode locked operation of the laser in the fundamental mode was obtained with the use of a $LiNbO_3$ phase modulator. A polarized output of about 0.4 watts was observed at a pulse rate of approximately 500×10^6 pps. Relatively stable mode locked operation of the laser was sustained for a period of a minute or two before readjustment of the system was required. Excessive loss of laser output due to polarization of the laser was noted. The loss is due to thermally induced stress birefringence, which is probably larger here than for the lamp pumped laser because of the large axial thermal gradient. Reduction of this gradient should result in lower polarization loss as well as higher TEM_{oo} mode power.

REFERENCES

1. L. Huff, "Sun Pumped Laser", Final Technical Report AFAL-TR-71-315.
2. W. Witte, "Cone Channel Optics", Infrared Physics, 1965, Vol. 5, pp. 179-185.
3. L. Huff and J. D. Taynai, "Space Laser Design", AF contract F33615-72-C-1629, final report to be submitted.
4. J. D. Foster and R. F. Kirk, "Space Qualified Nd:YAG Laser", Final Technical Report, NASA Contract NAS12-2160.
5. H. Kogelnik and T. Li, "Laser Beams and Resonators", Applied Optics, Vol. 5, pp 1550-1567, Oct. 1966.
6. J. Seffan, J. Lörtscher, and G. Herziger, "Fundamental Mode Radiation With Solid-State Lasers", IEEE JQE, Vol. QE-8, No. 2, pp 237-245, Feb. 1972.
7. R. B. Chesler and D. Maydan, "Convex-Concave Resonators for TEM_{oo} Operation of Solid-State Ion Lasers", J. Appl. Phys., Vol. 43, No. 5, pp 2254-2257, May 1972.
8. G. A. Massey, "Nd:YAlO Laser Device Research", AF Contract F33615-71-C-1650, final report to be submitted.
9. C. B. Hitz, "Frequency Doubled Modelocked Nd:YAG Laser", Final Report, NASA Contract No. NAS8-20967.

DOCUMENT CONTROL DATA - R&D

(Security classification of title, body of abstract and indexing annotation must be entered when the overall report is classified)

1 ORIGINATING ACTIVITY (Corporate author) GTE Sylvania Inc. - Electronic Systems Group Western Division, Electro-Optics Organization Mountain View, California 94040	2a. REPORT SECURITY CLASSIFICATION UNCLASSIFIED 2b. GROUP

3 REPORT TITLE

SUN PUMPED LASER

4. DESCRIPTIVE NOTES (Type of report and inclusive dates)

Final Report December 1971 to October 15, 1972

5. AUTHOR(S) (Last name, first name, initial)

Huff, Lloyd

6. REPORT DATE	7a. TOTAL NO. OF PAGES	7b. NO. OF REFS
September 1972	91	9

8a. CONTRACT OR GRANT NO. F33615-72-C-1240 b. PROJECT NO. c. d.	9a. ORIGINATOR'S REPORT NUMBER(S) 9b. OTHER REPORT NO(S) (Any other numbers that may be assigned this report) AFAL-TR-72-310

10. AVAILABILITY/LIMITATION NOTICES

[redacted]

11. SUPPLEMENTARY NOTES	12. SPONSORING MILITARY ACTIVITY Air Force Avionics Laboratory Wright-Patterson AFB, Ohio 45433

13 ABSTRACT

This report describes the results of a program to obtain improved operating performance of the sun pumped laser developed on the previous contract, AF contract F33615-70-C-1255. With more effective cooling of the laser rod, a nearly threefold increase in the multimode output power was achieved. A multimode output power of 4.85 watts was obtained with the 24 inch diameter collector using a copper heat sink which fully contacted the circumference of the laser rod. Operation of the device in a configuration compatible with dual sun and lamp or diode pumping, was also demonstrated. Operation of the sun pumped laser in the fundamental mode was obtained with the use of an intracavity lens to expand the beam within the laser rod. A TEM_{oo} output of 0.8 watts was obtained. Mode locked operation of the laser at a pulse repetition frequency of 500 MHz was also accomplished.

DD FORM 1 JAN 64 1473

14 KEY WORDS	LINK A		LINK B		LINK C	
	ROLE	WT	ROLE	WT	ROLE	WT
laser, sun mode locking space communications						

INSTRUCTIONS

1. ORIGINATING ACTIVITY: Enter the name and sddresa of the contractor, subcontractor, grantee, Department of Defense activity or other organization *(corporate author)* issuing the report.

2a. REPORT SECURITY CLASSIFICATION: Enter the overall security classification of the report. Indicste whether "Restricted Data" is included. Marking is to be in accordance with appropriate security regulstions.

2b. GROUP: Automatic downgrading is specified in DoD Directive 5200.10 and Armed Forces Industrial Manual. Enter the group number. Also, when applicable, show that optional markings have been used for Group 3 and Group 4 as suthorized.

3. REPORT TITLE: Enter the complete report title in all capital letters. Titles in all cases should be unclassified. If a mesningful title cannot be selected without classification, show title classification in all capitals in parenthesis immediately following the title.

4. DESCRIPTIVE NOTES: If appropriate, enter the type of report, e.g., interim, progress, summary, annual, or final. Give the inclusive dates when s specific reporting period ia covered.

5. AUTHOR(S): Enter the name(s) of author(s) as shown on or in the report. Entei last name, first name, middle initial. If military, show rank and branch of service. The name of the principal author is an absolute minimum requirement.

6. REPORT DATE: Enter the date of the report as day, month, year; or month, year. If more than one date appears on the report, use date of publication.

7a. TOTAL NUMBER OF PAGES: The total page count should follow normal pagination procedures, i.e., enter the number of pages containing information.

7b. NUMBER OF REFERENCES: Enter the total number of references cited in the report.

8a. CONTRACT OR GRANT NUMBER: If appropriate, enter the applicable number of the contract or grant under which the report was written.

8b, 8c, & 8d. PROJECT NUMBER: Enter the appropriate military department identification, such as project number, subproject number, system numbers, task number, etc.

9a. ORIGINATOR'S REPORT NUMBER(S): Enter the official report number by which the document will be identified and controlled by the originating activity. This number must be unique to this report.

9b. OTHER REPORT NUMBER(S): If the report has been assigned any other report numbers *(either by the originator or by the sponsor)*, also enter this number(s).

10. AVAILABILITY/LIMITATION NOTICES: Enter any limitations on further dissemination of the report, other than those imposed by security classification, using standard statements such as:

(1) "Qualified requesters may obtain copies of this report from DDC."

(2) "Foreign announcement and dissemination of this report by DDC is not authorized."

(3) "U. S. Government agencies may obtain copies of this report directly from DDC. Other qualified DDC users shall request through _____."

(4) "U. S. military agencies may obtain copies of this report directly from DDC. Other qualified users shall request through _____."

(5) "All distribution of this report is controlled. Qualified DDC users shall request through _____."

If the report has been furnished to the Office of Technical Services, Department of Commerce, for sale to the public, indicate this fact and enter the price, if known.

11. SUPPLEMENTARY NOTES: Use for additional explanatory notes.

12. SPONSORING MILITARY ACTIVITY: Enter the name of the departmental project office or laborstory sponsoring *(paying for)* the research and development. Include address.

13. ABSTRACT: Enter an abstract giving a brief and factual summary of the document indicative of the report, even though it may also appear elsewhere in the body of the technical report. If additional space is required, a continuation sheet shall be attached.

It is highly desirable that the abstract of classified reports be unclassified. Each paragraph of the abstract shall end with an indication of the military security classification of the information in the paragraph, represented as *(TS)*, *(S)*, *(C)*, or *(U)*.

There is no limitation on the length of the abstract. However, the suggested length is from 150 to 225 words.

14. KEY WORDS: Key words are technically meaningful terms or short phrases that characterize a report and may be used as index entries for cataloging the report. Key words must be selected so that no security classification is required. Identifiers, such as equipment model designation, trade name, military project code name, geographic location, may be used as key words but will be followed by an indication of technical context. The assignment of links, rules, and weights is optional.